# Intertidal Regions Regulate Seasonal Coastal Carbonate System Dynamics in the East Frisian Wadden Sea

Julia Meyer<sup>1, 3</sup>, Yoana G. Voynova<sup>1</sup>, Bryce Van Dam<sup>1</sup>, Lara Luitjens<sup>2</sup>, Dagmar Daehne<sup>2</sup>, Helmuth Thomas<sup>1, 3</sup>

- <sup>1</sup> Institute of Carbon Cycles, Helmholtz-Zentrum Hereon, Geesthacht, 21502, Germany
  - <sup>2</sup> Lower Saxony department of water management, coastal protection and nature protection (NLWKN), Norden, 26506, Germany
  - <sup>3</sup> Institute for Chemistry and Biology of the Marine Environment (ICBM), Carl von Ossietzky Universität Oldenburg, 26111 Oldenburg, Germany
- 10 Correspondence to: Julia Meyer (julia.meyer@hereon.de)

**Abstract.** Seasonal and regional changes in carbon dynamics in the Wadden Sea, the world's largest intertidal sand and mud flats system, were analysed to quantify the influence of biogeochemical processes on the carbonate system at the land-sea interface. With a focus on the East Frisian Wadden Sea (EFWS), we successfully used the difference between total alkalinity (TA) and dissolved inorganic carbon (DIC) ([TA-DIC]), as well as the calculated parameters ΔTA<sub>excess</sub>, ΔDIC<sub>excess</sub> (deviations beyond conservative mixing) and ΔTA<sub>P</sub> (alkalinity production linked to identify how ongoing primary production) to quantify local biogeochemical processes regulate theinfluences on carbonate system dynamics.

- In spring, a phytoplankton bloom with high biological activity, indicated by (a) supersaturated oxygen (up to 180 in % saturation), (b) elevated chlorophyll a (up to 151.7  $\mu$ g L<sup>-1</sup>) and (c) low  $pCO_2$  (as low as 141.3  $\mu$ atm), resulted in decrease in nitrate (NO<sub>3</sub><sup>-</sup>, 19.29  $\pm$  18.11  $\mu$ mol kg<sup>-1</sup>) and DIC (159.4  $\pm$  125.4  $\mu$ mol kg<sup>-1</sup>), and a slight increase in TA (9.1  $\pm$  29.2  $\mu$ mol kg<sup>-1</sup>).
- 20 The regression analysis of the differences between March and May 2022 (ΔMarch–May) in NO<sub>3</sub> concentrations (ΔNO<sub>3</sub>) against the differences in DIC (ΔDIC) yielded a slope of 6.90, matching the Redfield C:N ratio, and suggesting that uptake of nitrate by primary producers increased total alkalinity during the spring bloom.
  - In summer, we assume that organic matter remineralization, along with CaCO<sub>3</sub> dissolution in sediments, enhances TA production in the coastal and nearshore regions of the Western EFWS (up to 2400  $\mu$ mol kg<sup>-1</sup>). In the Eastern EFWS, enhanced CaCO<sub>3</sub> formation may consume TA ([TA-DIC] < 200  $\mu$ mol kg<sup>-1</sup>), but the region still acts as a net source of TA, likely due to sedimentary processes such as organic matter decomposition, which follow the time of increased biological activity during the spring bloom. The increase of TA enhances the coastal ocean's ability to absorb and store CO<sub>2</sub> through buffering and suggests that the EFWS can be a source of TA to the coastal regions during the warm productive seasons. This study highlights the complex relationships between these factors, emphasizing the need for a comprehensive understanding of regional and seasonal
- 30 variations to better assess the role of coastal systems in carbon cycling, and storage, and climate regulation.

#### 1 Introduction

35

40

45

Coastal oceans are biogeochemically active regions, which play a significant role in biogeochemical cycles, despite covering less than 10 % of the oceanic realm (Gattuso et al., 1998). Coastal regions are directly affected by terrestrial organic matter and nutrients through river run-off, groundwater discharge, atmospheric deposition, and exchange of large amounts of matter and energy with the open ocean (Borges et al., 2006; Gattuso et al., 1998). Overall, coastal oceans also support approximately 14 - 23 % of the ocean carbon dioxide uptake, 10 - 30 % of the primary production, 80 % of organic matter burial, 90 % of sedimentary mineralization and 75 - 90 % of the oceanic sink of suspended river loads (Bauer et al., 2013; Gattuso et al., 1998). Since the start of the industrial era, the levels of CO<sub>2</sub> in the atmosphere have increased from ~280 ppm to over ~419 ppm due to human activities (Friedlingstein et al., 2023). About 30 % of anthropogenic CO<sub>2</sub> emissions since the industrial period have been absorbed by the ocean (Friedlingstein et al., 2023). The uptake increases the concentration of protons [H<sup>+</sup>] and decreases the carbonate ion concentration [CO<sub>3</sub><sup>2-</sup>], leading to lower pH and a reduced saturation state of calcium carbonate, a process known as ocean acidification (Orr et al., 2005). Depending on the different model scenarios, it is predicted that surface pH in the ocean might decline by about 0.3 - 0.4 pH units by 2100, corresponding to a decrease of about 40 - 50 % of carbonate ions in the seawater (Feely et al., 2009; Orr et al., 2005). The future capacity of the ocean to take up CO<sub>2</sub>, can affect the precipitation and dissolution of the carbonate minerals, as well as the survival of marine organisms (Duan et al., 2023; Kroeker et al., 2013; Liang et al., 2023; Ricour et al., 2023). Whereas oceans are a significant sink for anthropogenic CO<sub>2</sub> it is not well known how this uptake will further change under the continual increase of anthropogenic CO<sub>2</sub> in the atmosphere (Lorkowski et al., 2012; Sabine et al., 2004; Thomas et al., 2007). However, rising atmospheric CO<sub>2</sub> will influence carbon stocks and fluxes in the pelagic, benthic and coastal zone, particularly in shelf seas, which are annually mixed and ventilated (Legge et al., 2020). Total alkalinity (TA) represents the buffering capacity of the ocean and is controlled by many factors including erosion/weathering pathways on land (Lehmann et al., 2023) and respiration of organic matter (OM) along anaerobic metabolic pathways, mostly generated in shallow marine and shelf sediments (Dickson, 1981). These processes are directly influenced by terrestrial and anthropogenic nutrient inputs (Van Beusekom and De Jonge, 2002; (Burt et al., 2016; Thomas et al., 2009); Van Beusekom & De Jonge, 2002), as well as increased sedimentation of reactive organic matter (OM) (Al-Raei et al., 2009; Böttcher et al., 1998a) 1998). Coastal seas and shelf seas, like the North Sea often have relatively high rates of primary production in spring, leading to drawdown in DIC,  $pCO_2$  and a consequent pH increase (Macovei et al., 2021; Thomas et al., 2005). In addition, nutrient loads from land contribute to enhanced primary production, and increased carbon remineralization (Prowe et al., 2009; Thomas et al., 2009), and subsequent changes in the carbonate system. Previous studies suggested that the Wadden Sea, a large network of intertidal sand and mudflats bordering the North Sea along the Dutch, German and Danish coasts (Staneva et al., 2009), plays a significant role in modulating local carbonate system dynamics (Thomas et al., 2009; Voynova et al., 2019)... The seasonal TA production in the southern North Sea, exhibited a regional TA variability, which was

attributed to the influence of the Wadden Sea (Voynova et al., 2019), and to benthic TA production (Brenner et al., 2016).

The observed seasonal changes of TA can affect the coastal ocean capacity to absorb carbon from the atmosphere (Burt et al., 2016; Gruber et al., 2019; Li et al., 2024; Schwichtenberg et al., 2020).

This study offers a detailed analysis of seasonal and inter-annual carbonate system dynamics in the EFWS, a key region within the world's largest intertidal sand and mudflat system (UNESCO World Heritage Centre, n.d.). As an essential component of coastal carbon cycling, and a land sea junction, this area requires a deeper understanding of the processes influencing TA and DIC. The research focuses on seasonal and regional variations, and particularly on the drivers of TA production in spring-summer. By examining changes in TA, DIC, and other biogeochemical parameters, this study identifies key mechanisms affecting carbonate chemistry, including calcium carbonate (CaCO<sub>3</sub>) dissolution and formation, photosynthesis and respiration. Our findings highlight the complex interactions among these factors, emphasizing the need for a comprehensive understanding of regional and seasonal variations to better assess the role of coastal systems in carbon cycling, storage, and climate regulation. Moreover, observed TA and DIC distributions provide valuable insights into potential carbon and TA sources within this dynamic environment.

#### 2 Material and Methods

#### 2.1 Study Side

75

The German Bight region is bordered by Germany, Denmark and the Netherlands, situated in the southeastern corner of the North Sea (Fig. 1a). The East Frisian Wadden Sea (EFWS) is one of the shallowest regions of the German Bight, characterized by a series of barrier islands (Fig. 1b), each 5—\_17 km long and 2—\_3 km wide (Staneva et al. 2009). The system is an intertidal region, influenced by semidiurnal tides with a tidal range from approximately 2.2—2.8 m (Grunwald et al. 2009; Staneva et al. 2009) and up to ~ 3.5 m in the Elbe River mouth (Staneva et al. 2009). —2.8 m (Grunwald et al. 2009; Staneva et al. 2009) and up to ~ 3.5 m in the Elbe River mouth (Staneva et al. 2009). Main freshwater sources to the German Bight are the rivers Elbe, Weser, and Ems, with additional river discharge values of 860 m³ s⁻¹ (Elbe), 323 m³ s⁻¹ (Weser), and 80 m³ s⁻¹ (Ems) (Luebben et al., 2009; Schmidt et al., 2011 and references herein). However, model estimates indicate that only about 5% of the TA variability in the German Bight is attributable to effective river loads (Schwichtenberg et al., 2020). Seasonally, the river inflow and hydrodynamics can affect the carbonate system in the German Bight. During winter, high freshwater input (e.g., Elbe ~1420 m³ s⁻¹ in February) leads to reduced salinities, whereas in summer discharge is considerably lower (e.g., Elbe ~300 m³ s⁻¹ in August), resulting in comparatively more marine conditions (Rewrie et al., 2023; Schwichtenberg, 2013; Schwichtenberg et al., 2020; Voynova et al., 2017).

The study site is also characterized by complex local freshwater dynamics. Local sluices (e.g., in Greetsiel, Bensersiel, Harlesiel, Carolinensiel, or Neuharlingersiel) regulate freshwater inflow in intertidal regions and can thereby affect salinity levels and nutrient dynamics in the Wadden Sea (Luebben et al., 2009). The opening of such sluices is primarily controlled by tidal cycles but can also vary seasonally depending on precipitation and drainage needs. As shown by Beck et al. (2012)

freshwater discharged through a sluice along the East Frisian coast, can be enriched in terrestrial organic matter and trace metals and undergoes strong geochemical modifications upon mixing with seawater. Such processes, comparable to those in estuaries, are likely to influence not only trace metal dynamics but also carbonate chemistry and nutrient availability in the Wadden Sea. Terrestrial run-off enters the back-barrier tidal flats of Spiekeroog via the sluice located in Neuharlingersiel (Fig. 1b), generally about 2 h before low tide when the water level of the hinterland is above sea level, with drainage volume depending on precipitation in the catchment area (ca. 125 km²) and averages 15 × 106 m³ in winter and 9 × 106 m³ in summer (Luebben et al., 2009 and references therein).

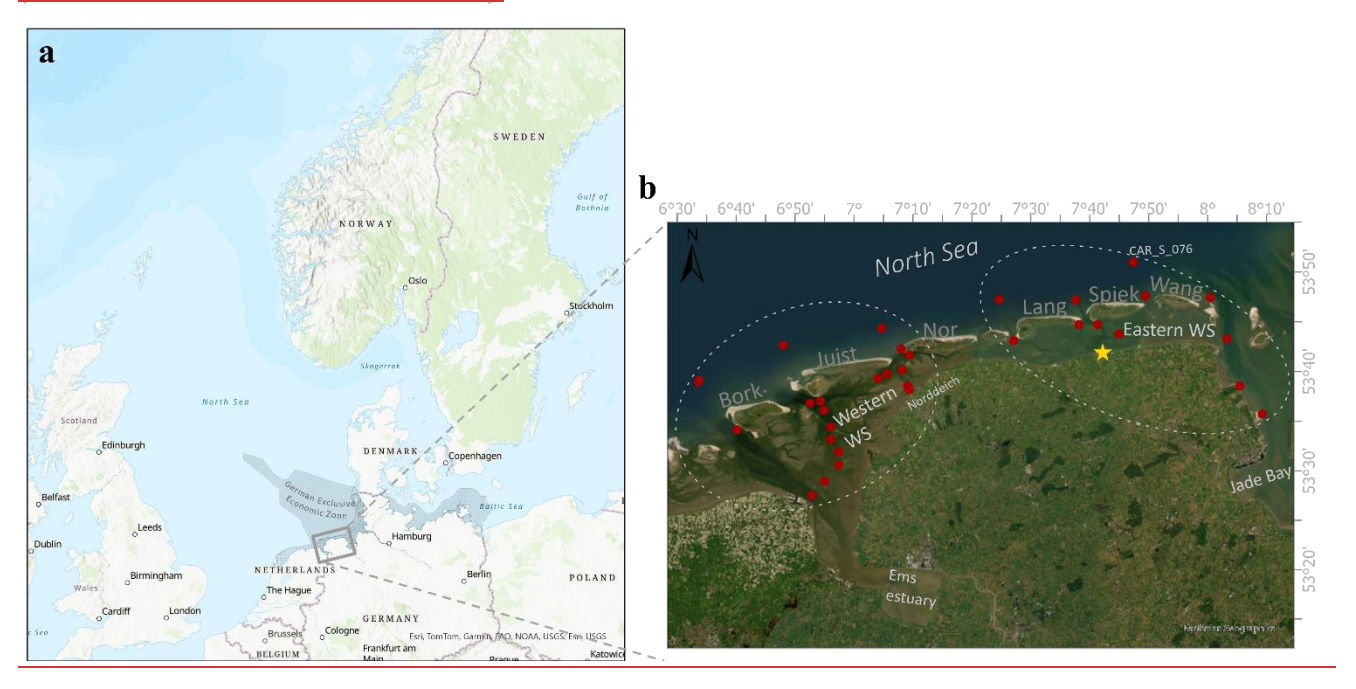


Figure 1: Study area, (a) The German Wadden Sea (=WS), (shown in grey) with the German Exclusive Economic Zone (hatched region) and the East Frisian Wadden Sea (EFWS) region (grey box). (b) Zoom into the EFWS, showing the sampling stations (red dots) in the different regions (Western WS and Eastern WS) considered in this study. The yellow star shows the Neuharlingersiel sluice location. Station CAR S 076, used as the North Sea endmember, is explicitly labelled (see section 2.5). The different Islands are labelled with the first few letters of their names (Bork= Borkum, Juist, Nor= Norderney, Lang= Langeoog, Spiek= Spiekeroog, Wang= Wangeoog). The map in this Figure was generated using ArcGIS. Data sources: (a) Esri, TomTom, Garmin, FAO, NOAA, USGS; (b) Earthstar Geographics. © 2024 Julia Meyer.

We separated the study area ininto two regions (Western WS & Eastern WS; Fig. 1b) due to the differences in the tidal dynamics and hydrodynamic properties (Herrling and Winter, 2015), which drive the area's carbon dynamics, sediment transport, and overall ecological functioning. The tidal range increases from 2.4 m at Borkum to 3.0 m at Wangerooge, with the Eastern region experiencing stronger tidal influences (Herrling and Winter, 2015). In the Langeoog basin, wind effects cause the largest relative increase in residual discharge, while Norderney experiences the largest absolute increase in water flux. Westerly winds influence residual circulation and sediment transport differently in each region. The flow dynamics between the basins of Baltrum and Langeoog are interconnected, whereas the flow regime between Borkum and Norderney is more independent from the dominant circulation patterns and inter-basin exchange (Herrling and Winter, 2015).

Seasonal cruises were completed in the Wadden Sea (WS) and North Sea around the East Frisian Islands (and the Ems River estuary) with the research vessel (RV) *Burchana* (Lower Saxony department of water management, coastal protection, and 90 nature protection (NLWKN; Fig. NLWKN; Fig. 1b). The July 2021 and October 2021 cruises focused exclusively on the intertidal mudflats of the EFWS. The RV *Burchana*, with a draft of 1.3 meters, allowed sea water sampling even during low tide, providing the opportunity to collect samples at various tidal stages. Sampling took place during daylight hours, typically starting in the morning at low tide and continuing throughout the day, with no nighttime samples collected. Both shallow intertidal areas (accessible due to the vessel's low draft) and deeper subtidal channels were sampled to ensure comprehensive spatial coverage. Later cruises extended into the Ems River Estuary, from the island of Borkum (Bork, Fig. 1b) to Weener (53°09'55.4"N 7°20'39.9"E), a town located upstream the Ems River Estuary. These additional data from the Ems River will be presented in a subsequent paper.

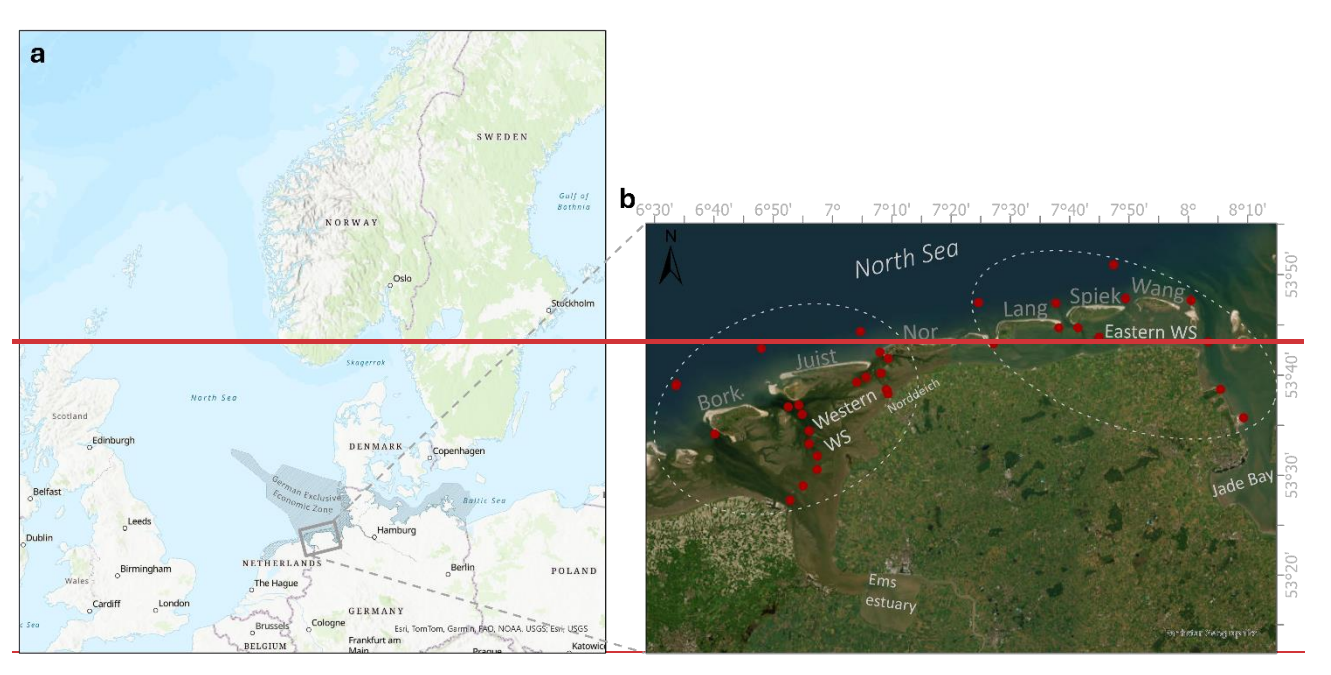


Figure 1: Study area, (a) The German Wadden Sea (-WS), (shown in grey) with the German Exclusive Economic Zone (hatched region) and the EFWS region (grey box). (b) Zoom into the EFWS, showing the sampling stations (red dots) in the different regions (Western WS and Eastern WS) considered in this study. The different Islands are labelled with the first few letters of their names (Bork= Borkum, Juist, Nor= Norderney, Lang= Langeoog, Spick= Spickeroog, Wang= Wangeoog). The map in this Figure was generated using AreGIS. Data sources: (a) Esri, TomTom, Garmin, FAO, NOAA, USGS; (b) Earthstar Geographics. © 2024 Julia Meyer.

## 2.2 FerryBox measurements

135

120

A FerryBox system (4H-JENA engineering GmbH, Jena, Germany) was operated during all cruises on board the *RV Burchana* (NLWKN), measuring the following parameters every minute: temperature (SBE38, Sea-Bird Scientific, <u>USA</u>), salinity (SBE45, Sea-Bird Scientific, <u>USA</u>), dissolved oxygen (DO) (Optode 4835, Aanderaa, Bergen, Norway), chlorophyll

fluorescence to estimate chlorophyll a concentrations (AlgaeOnlineAnalyser, bbe moldaenke, Germany), pH (electrode, Xylem; measured on total scale, USA) and turbidity (Solitax inline SC, Hach Lange, Germany). The pH electrode was calibrated using standard DuraCal buffer solutions at pH 7 and pH 10 (Hamilton Company, USA). The partial pressure of CO<sub>2</sub> (pCO<sub>2</sub>) was measured using a sensor (HydroC CO<sub>2</sub>-FT, 4H-JENA engineering, Germany) attached to the flow-through system of the FerryBox. The These data were corrected using the data processing manual of 4H - Jena Engineering GmbH (4H Jena, 2021). Regions near the ports were excluded in all datasets, to remove any influence from the port, or from the cleaning cycles.

### 145 **2.3 Discrete samples**

140

160

165

170

Samples for Winkler titration (dissolved oxygen), nutrients, salinity and turbidity were collected from each cruise to crosscheck the measurements of the FerryBox. Therefore, dissolved oxygen (DO) samples were collected on the last day of each cruise by filling Biological Oxygen Demand (BOD) bottles from the FerryBox outflow. Three replicates collected underway were treated according to the standard Winkler method and measured within 24 hours in the lab using a Metrohm 870 KF Titrino Plus- (Germany). The Winkler titrations were used to correct the FerryBox dissolved oxygen measurements from the seasonal cruises. A single regression equation forof the Winkler titrations and the FerryBox data was used to apply a dissolved oxygen correction of the entire data set (y= 1.17x - 31.89, R<sup>2</sup>= 0.98, n= 46). Here, x is the measured raw data of the FerryBox optode in umol L<sup>-1</sup>, and y is the corrected dissolved oxygen value based on Winkler titrations, also in umol L<sup>-1</sup>.

In addition, the apparent oxygen utilization (AOU) was calculated using the corrected oxygen measurements, as according to:

155 
$$AOU = O_2 - O_2$$
 (1)

Where  $O_2$ ' is the expected oxygen in  $\mu$ mol  $L^{-1}$ at equilibrium with the atmosphere, at the measured temperature and salinity according to Grasshoff et al., (1999), and  $O_2$  is the oxygen concentration measured by the FerryBox optode.

Duran bottles (~ 300 mL) were filled with sample water during all seasonal cruises using the FerryBox outflow to measure turbidity and salinity in the laboratory. Salinity was measured using an OPTIMARE High Precision Salinometer (Optimare Systems GmbH, Bremerhaven, Germany) and turbidity was measured using a Hach 2100 turbidimeter.

Nutrient samples were collected at each station using the onboard water sampler. A sample volume of 250 mlmL was filtered through pre-combusted GF/F filters, and the samples were collected in clean centrifuged tubes, frozen and stored at -20 °C. The concentrations of nitrite (NO<sub>2</sub><sup>-</sup>), nitrate (NO<sub>3</sub><sup>-</sup>) ammonium (NH<sub>4</sub><sup>+</sup>) and silicate (SiO<sub>2</sub>) were also measured using a MicroMaC analyser from SYSTEA (Anagni (FR), Italy). The system, which induces a colour reaction, is coupled with a photometer (NO<sub>2</sub><sup>-</sup>, NO<sub>3</sub><sup>-</sup>, SiO<sub>2</sub>) and a fluorometer (NH<sub>4</sub><sup>+</sup>), using a one-point calibration. NO<sub>3</sub><sup>-</sup> was determined with sulfanilamide and N- (1- Naphthyl)ethylenediamine, NH<sub>4</sub><sup>+</sup> with orthophthalaldehyde and NO<sub>2</sub><sup>-</sup> with diethylenetriaminepentaacetic acid and automatic UV reduction (Luitjens, 2019).

Water samples for TA and DIC were collected in 300 mL BOD bottles at all stations using the FerryBox outflow according to the Standard Operating Procedure (SOP) (Dickson et al. 2007). The samples were poisoned with saturated mercury chloride and measured in the laboratory with a VINDTA 3C (MARIANDA, Kiel, Germany), using certified reference material (CRM) (Dickson et al. 2003). The method is precise, with a reproducibility better than 1 µmol kg<sup>-1</sup> and an accuracy within 2 µmol kg<sup>-1</sup>

(Dickson et al. 2003). The results within this study were plotted with R Project (ggplot package) and maps were created with ArcGIS Pro. In addition, the saturation state of calcite (Ωcal) calculated using the CO2SYS program developed by (Lewis et al. 1998) with CO2 solubility constants of Lucker et al. (2000).

In addition, the saturation state of calcite (Ωcal) was calculated using the CO2SYS program developed by (Lewis & Wallace, 1998). The dissociation constants for carbonic acid (K<sub>1</sub> and K<sub>2</sub>) were taken from Lueker et al. (2000), which are widely used for seawater CO<sub>2</sub> chemistry and generally provide reliable results, with uncertainties in K<sub>1</sub> and K<sub>2</sub> translating to about ±1 % in calculated *p*CO<sub>2</sub>. For bisulfate (KHSO<sub>4</sub>), the constant of (Dickson, 1990) was applied, and for the boron-to-chlorinity ratio of Lee et al. (2010).

## 2.4 [TA-DIC] as a proxy for Biogeochemical Processes Processing

180

185

195

200

[TA-DIC] is a good proxy for biogeochemical processes such as CaCO<sub>3</sub> precipitation / formation, photosynthesis, respiration and therefore CO<sub>2</sub> uptake and release, even in coastal oceans (Xue and Cai, 2020). The parameter is independent of ocean mixing and not sensitive to temperature and pressure changes, and this makes it a good tracer for larger-scale oceanographic studies, and suitable for seasonal observations of biogeochemical processes and carbonate dynamics of an ecosystem. In addition, it is assumed that [TA-DIC], can better reflect variations of [CO<sub>3</sub><sup>2-</sup>] compared to the ratio of TA and DIC (Xue et al., 2017).

The difference between TA and DIC is often expressed as:

$$[TA - DIC] = TA - DIC$$
 (2)

However, [TA–DIC] should not be used at low salinity (e.g. <20) and when [TA–DIC] is < ~50 μmol kg<sup>-1</sup>, where the relationships of [TA–DIC] with pH and/or ocean acidification are nonlinear, these low values also occur in oxygen minimum zones (Xue and Cai 2020).

#### 2.5 Calculations of estuarine DIC and TA contributions

To estimate the contributions of estuarine DIC and TA in the Western and Eastern EFWS, we used DIC and TA measurements from the lowest salinity station located in the Wadden Sea, just before the Ems Estuary (where the Emsriver enters the Wadden Sea) as endmembers for our mixing model. The stations chosen for these measurements were in areas of low salinity within the estuary, with considerable influence of freshwater (influence (DIC<sub>estuary</sub>; TA<sub>estuary</sub>; Table 1). These values (DIC<sub>estuary</sub>; TA<sub>estuary</sub>) were used to calculate the DIC<sub>mixing w/Rest</sub> and TA<sub>mixing w/Rest</sub> (equation 3 and 4) for the different regions. We hereafter denote these conservative mixing values as DIC<sub>mixing w/est</sub> and TA<sub>mixing w/est</sub>, i.e. the expected concentrations under two-endmember mixing between the North Sea (Wadden Sea) and estuarine sources.

Table 1: DIC<sub>estuary</sub>, DIC<sub>NorthSea</sub>, S<sub>NorthSea</sub>, TA<sub>estuary</sub> and TA<sub>NorthSea</sub> used for the calculation of the seasonal DIC<sub>mixing w/R</sub> concentrations of each season.

Season and Region	DICNorthSea	DICestuary	SNorthSea	TANorthSea	TAestuary
-------------------	-------------	------------	-----------	------------	-----------

July 2021	2144. <del>07</del> <u>1</u>	2261. <del>20</del> 2	31. <del>79</del> <u>8</u>	2273. <del>70</del> 7	2465. <del>12</del> 1
October 2021	2188.4 <u>6</u> 5	2224. <del>90</del> 9	<del>30.97</del> <u>31.0</u>	2369. <del>27</del> <u>3</u>	2411. <del>68</del> <u>7</u>
March 2022	2205. <del>66</del> 7	2238. <del>05</del> 1	31. <u>475</u>	2338. <del>37<u>4</u></del>	2318. <del>90</del> 9
May 2022	2199. <del>86</del> <u>9</u>	2205. <del>52</del> <u>5</u>	32. <u>131</u>	2332.49 <u>5</u>	2447. <del>76</del> <u>8</u>
July 2022	2144.41 <u>4</u>	2310. <del>22</del> 2	31. <del>78</del> <u>8</u>	2356. <del>59</del> <u>6</u>	2489. <u><del>56</del>6</u>

In this study, DIC<sub>NorthSea</sub> (and TA<sub>NorthSea</sub>) refers to the DIC (and TA) values at the station (CAR\_S\_076) located farthest from land behind Spiekeroog and Wangeoog (Fig. 1b), which we used as our marine North Sea endmember, as it is situated farthest offshore of the Ems and experiences the highest salinity (S<sub>NorthSea</sub>) levels during almost each season. The DIC<sub>NorthSea</sub> and TA<sub>NorthSea</sub> endmembers applied for each season are shown in Table 1.

Starting with from these endmembers, we used the expected DIC and TA at each station due to conservative mixing were calculated following the equations of Jiang et al. (2008) and Joesoef et al. (2015) to calculate the contribution of riverine DIC and TA:

$$\frac{\text{DIC}_{\text{mixing w/R}}}{\text{DIC}_{\text{mixing w/est}}} = \frac{s_i}{s_{\text{NorthSea}}} * \text{DIC}_{\text{NorthSea}} + (1 - \frac{s_i}{s_{\text{NorthSea}}}) * \text{DIC}_{\text{estuary}}$$

(3

205

210

$$\frac{TA_{\text{mixing w/R}}TA_{\text{mixing w/est}}}{S_{\text{NorthSea}}} * TA_{\text{NorthSea}} + (1 - \frac{S_i}{S_{\text{NorthSea}}}) * TA_{\text{estuary}}$$
(4)

where  $S_i$  represents the salinity at each related station *i*. The ratio  $\frac{S_i}{S_{NorthSea}}$  normalizes the influence of the salinity at the specific station by the salinity of the North Sea ( $S_{NorthSea}$ ).

In addition, To quantify the net contributions of estuarine processes beyond conservative mixing, ΔDIC<sub>excess</sub> was and ΔTA<sub>excess</sub> were calculated to estimate the contribution due to estuarine input in the different regions. Therefore, using the equation of (Jiang et al., 2008; Van Dam et al., 2018) was used:

$$\Delta DIC_{\text{excess}} = DIC_i - \frac{DIC_{\text{mixing w/R}}}{DIC_{\text{mixing w/est}}}$$

(5)

$$220 \quad \Delta TA_{\text{excess}} = TA_i - \frac{\text{This equation includes}}{\text{TA}_{\text{mixing w/est}}}$$

(6)

These calculations use the measured DIC and TA concentrations of the related at station *i*-and, together with the DIC mixing w/R-of equation 5. ΔTA mixing w/R-and ΔTA excess were calculated the same way with the est and TA mixing w/est values from equations 3 and 4. Here, ΔDIC excess represents the deviation of the measured TA of each station using the TA estuary, TA NorthSea values (Table 1): DIC from the expected conservative mixing value, while ΔTA excess = TA TA mixing w/R.

(6)

ADIC<sub>excess</sub> and  $\Delta TA_{excess}$  quantifies the corresponding deviation for TA. Values close to zero indicate that concentrations were calculated to remove are consistent with mixing alone. Positive or negative deviations reflect local biogeochemical processes

(e.g., photosynthesis, respiration, carbonate precipitation or dissolution) or additional inputs and losses not represented by the two endmembers. By accounting for conservative mixing, this approach isolates the influence of biogeochemical processes and external contributions from the physical mixing effect of water masses from the estuary outflow with the North Sea, as the coastal region of the EFWS is closely connected to the land. A ΔDIC excess value of approximately zero means that the DIC is not different than what would be expected from mixing between the North Sea and estuarine outflow waters. Negative values of ΔDIC excess indicate that the DIC consumption exceeded production in this area, which reduces DIC or, equivalently increases ΔTA excess. Positive values of ΔTA excess suggests higher values than expected based on mixing alone, indicating TA sources. Therefore, during During productive seasons, primary production will decrease DIC, while consuming CO<sub>2</sub> and nutrients (Xue & Cai, 2020). The uptake of NO<sub>3</sub><sup>-1</sup> can increase TA, while the uptake of NH<sub>4</sub><sup>+1</sup> can decrease TA in an ecosystem (Brewer & Goldman, 1976; Wolf-Gladrow et al., 2007). The production of 1 mol organic matter ((CH<sub>2</sub>O)<sub>106</sub>(NH<sub>3</sub>)<sub>16</sub>H<sub>3</sub>PO<sub>4</sub>) will generally increase TA by 17 mol TA (ΔTA<sub>P</sub>) and decrease DIC by 106 mol and will change the TA and DIC concentrations (Chen, 1978). Consequently, ΔTA<sub>P</sub> is used to calculate the expected amount of TA produced, according to the equation of ΔTA<sub>bio</sub>

$$\Delta TA_P = \frac{-17/106 * \Delta DIC_{excess}}{(7)} (-17/106) * \Delta DIC_{excess}$$

It is important to note, that the calculation of ΔTA<sub>P</sub> is an overestimation assuming the measured TA is modulated by photosynthesis (NO<sub>3</sub><sup>-</sup> - fueled fuelled) or respiration, such that the presence of other non-photosynthetic DIC sinks will cause ΔTA<sub>P</sub> to be overestimated.

#### 3 Results

230

235

240

#### 3.1 Regional and seasonal variation in the East Frisian Wadden Sea EFWS

from (Xue and Cai 2020), which was modified using the calculated ΔDIC<sub>excess</sub>:

In July 2021, salinities were lowest on the route from Norddeich harbour to Norderney (25.2), and around Norderney (Table 2; Fig. S1) in the Western WS- (Table 2; Fig. S1). In summer 2022, the salinity on July 12 (31.16 - 32.03) increased by 2 - 3 salinity units compared to July 11 (28.28 - 29.43) in the Eastern WS (Table 2; Fig. S1). This indicates that during July 2022 cruise, there was a change in salinity range between the first and second leg of the cruise (in roughly the same region). A possible reason for these salinity differences could be the Neuharlingersiel sluice opening in the early morning of July 11, 2022, which could have influenced the salinity on this day. The turbidity in October 2021 showed a completely different pattern compared to all other seasons, with values from 96.08 – 306.46 NTU (Fig. S1), caused by rougher weather conditions during the campaign.

A land\_to\_sea gradient <u>in pH</u> was observed in <del>pH in October 2021 (Fig. S2), which varied from 7.6 to \_8.1 (; Table 2). Higher ; Fig. S2), with higher values were measured in the North Sea offshore regions (behind Juist, Norderney, Langeoog), whereas the and lower values were measured closer to near the mainland coast. Regional differences with maximum pH values of >> 28</del>

in the higher\_salinity waters were measured during observed in all seasons (Fig. S2; Table 2), with pH > 8particularly high values in the Western WS, in front of Norderney-Wadden Sea in May 2022 (Fig. S2; Table 2).
 The maximum concentrations of chlorophyll a were observed in May 2022, displaying the most substantial fluctuations (Table 2), especially in the Western part (up to 151.7 μg L<sup>-1</sup>) (Fig. S2). In July 2021, the highest chlorophyll measurements (up to 74.7 μg L<sup>-1</sup>) were detected underway between Norderney to Spickeroog (Table 2; Fig. S2). A similar pattern can be seen
 for July 2022 (Fig. -S2), although measurements were not available for all transects.

Table 2: Overview of the different measured parameters: Temperature (°C), Salinity, pH, oxygen (% saturation), AOU ( $\mu$ mol L<sup>-1</sup>), Chlorophyll a (Chl a in  $\mu$ g L<sup>-1</sup>), pCO<sub>2 obs</sub> ( $\mu$ atm) and Calcite saturation  $\Omega$ cal of all seasonal samplings in the EFWS.

Parameter	July 2021	October 2021	March 2022	May 2022	July 2022
Temperature (°C)	18.59 - 23.15	12.66 – 16.57	3.89 - 6.47	9.65 – 18.19	17.36 – 21.04
Salinity	25.21 - 32.33	25.21 – 31.32	18.32 - 31.97	23.59 - 32.28	23.35 - 32.04
рН	7.71 - 8.16	7.64 - 8.13	7.66 - 8.13	7.95 - 8.55	7.71 - 8.08
Oxygen (% sat)	$109.7 \pm 9.5$	$100.9 \pm 5.3$	$105.5 \pm 3.1$	$132.9 \pm 13.0$	$102.4 \pm 5.2$
AOU (μmol L-1)	$-22.7 \pm 22.2$	$-2.3 \pm 14.4$	$-17.5 \pm 10.0$	$-88.9 \pm 33.9$	$-5.3 \pm 12.4$
Chl a (µg L-1)	$25.6 \pm 12.9$	$16.9 \pm 8.9$	$13.4 \pm 6.5$	$52.1 \pm 29.4$	$23.2\pm19.3$
pCO <sub>2 obs</sub> (µatm)	_	$521.6 \pm 72.2$	$468.2 \pm 54.5$	$269.0 \pm 63.7$	$536.0 \pm 116.5$
Ωcal	$3.8 \pm 0.9$	$3.21 \pm 0.6$	$2.5 \pm 0.4$	5.2 ± 1.1	$3.7 \pm 0.4$

270

280

285

The maximum concentrations of chlorophyll a were observed in May 2022, displaying the most substantial fluctuations (Table 2), especially in the Western part from Norderney to Borkum (up to 151.7 μg L<sup>-1</sup>) (Fig. S2). In July 2021, the highest ehlorophyll measurements (up to 74.7 μg L<sup>-1</sup>) were detected underway between Norderney to Spiekeroog (Table 2; Fig. S2). A similar pattern can be seen for July 2022 (Fig. S2), however no measurements from Norderney to Spiekeroog are available for chlorophyll a. This is also the case for October 2021 from Norderney to Wangeoog (Fig. S2).

In July 2021 the measured oxygen ranged from 72.4 – 112.01 in % saturation (Fig. S2), with the highest values in the Wadden Sea of Langeoog. Western WS. Oxygen decreased from July 2021 to October 2021, on average by 8.8 ± 10.9 % saturation (Table 2; Fig. S2). The lowest oxygen saturation was measured from Norddeich to Norderney in October (down to ~ 57 % saturation). Until May, oxygen Oxygen saturation then increased continuously over the year. The highest oxygen (until May, reaching maximum values up to ~ 180 % saturation) was measured in May in the intertidal region of Norderney in the Western EFWS and around Wangeoog in the Eastern EFWS (up to ~ 152 % saturation) (in the Eastern EFWS (Table 2; Fig. S2).

Overall, oxygen decreased by a mean value of  $28.4 \pm 16.4$  % saturation from May to July 2022 (Fig. S2), resulting in slightly lower oxygen saturation in July 2022 compared to the previous year (Table 2). For the AOU (Table 2), the same inverse picture was obtained. The observed  $pCO_2$  ( $pCO_2$  obs) was highest in July 2022 and lowest in May 2022 (down to 141.3  $\mu$ atm) in the Western WS. The average decrease in  $pCO_2$  obs was  $166.2 \pm 276.1$   $\mu$ atm from March to May 2022 (Table 2; Fig. S3).

During all seasons,  $\Omega$ cal was supersaturated, ranging from 1.5 – 7.5 (Table 2), but with a pronounced seasonal pattern. Higher, supersaturated  $\Omega$ cal values (> 2.5) were observed during more productive seasons (July 2021, July 2022, May 2022). However,

the highest variability of  $\Omega$ cal was found in May 2022 with values > 1 in 80 % of the stations and reaching up to 7.52 in the WS of Juist and BorkumWesern WS (Table 2; Fig. S3). In summer (July 2021, July 2022), a decrease of  $\Omega$ cal in the EFWS from West to East was observed, regionally (Fig. S3).

## 3.2 TA and DIC Variability in the East Frisian Wadden Sea EFWS

290

295

300

305

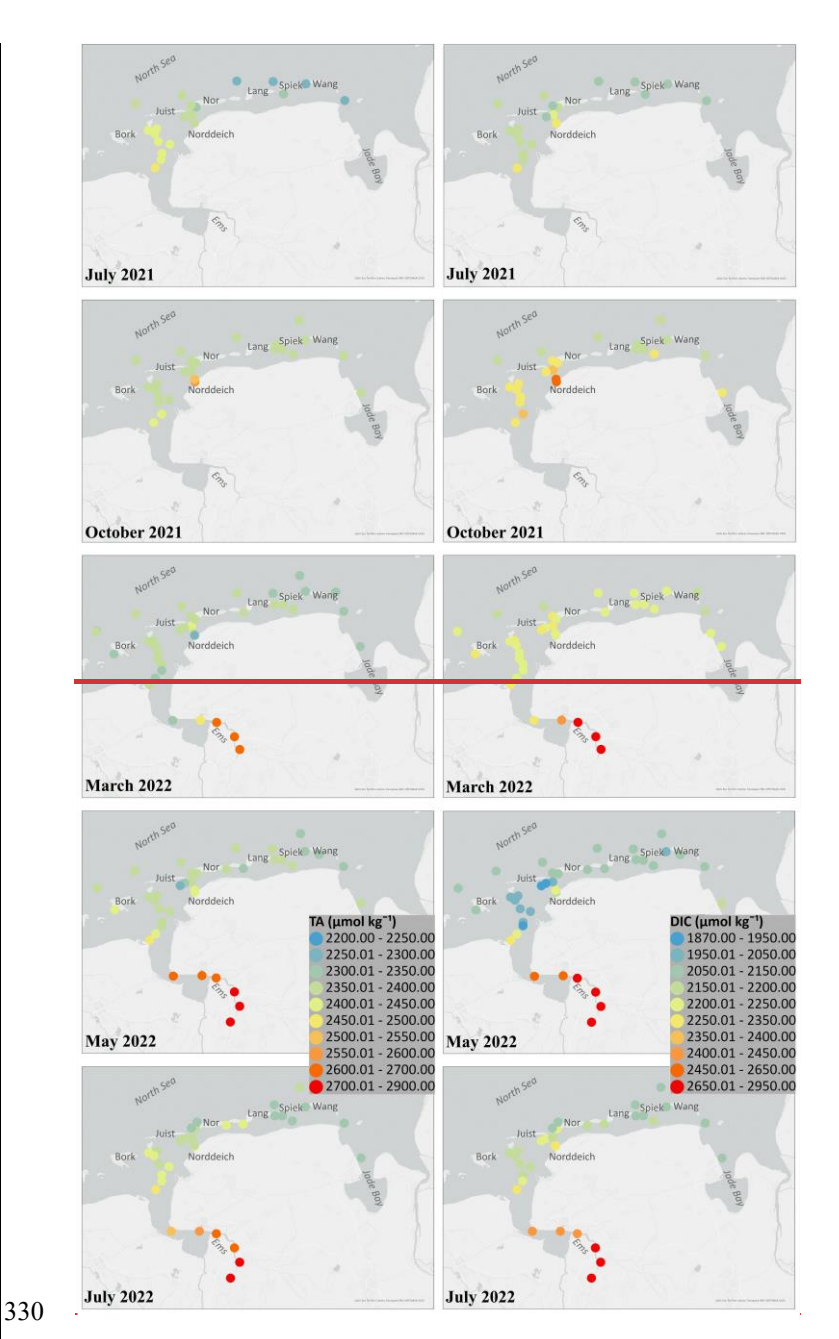
Large seasonal and regional variability in DIC and TA and DIC was observed, seasonally but also regionally along the estuarine land to—sea gradient inof the EFWS (Table 3; Fig. 2)), with particularly high TA values in summer (Table 3; Fig. 23b). In July 2021, TA ranged from ~2273 μmol kg<sup>-1</sup> μmol kg<sup>-1</sup> in the Jade Bay (Eastern WS) and increased regionally westward (up to—to ~2465 μmol kg<sup>-1</sup>) to Norderney (Table 3; Fig. 2; Fig. μmol kg<sup>-1</sup>, following a negative 3a)- All measured TA values were above or slightly below the mixing line with a negative slope (—of –24.9 μmol kg<sup>-1</sup>9 μmol kg<sup>-1</sup> per salinity unit) (Fig. 3a), indicating (Fig. 3b). Most data points were close to or slightly above this line, consistent with net TA production- in this tidally driven system. In July 2022, TA was lower TA values were measured during the first leg of the cruise whenat reduced salinities were lower (28—29) (Table 3; Fig. 2; Fig. 3a), but ain the Eastern WS, although the slope versus salinity remained similar slope (—(23.3 μmol kg<sup>-1</sup>3 μmol kg<sup>-1</sup> per salinity unit) of the short). At higher salinities (31–32) in the Western WS, values were comparable to July 2021, again closely following the conservative mixing line was observed (Fig. 3a). At higher salinity stations in July 2022 (up to 32), TA values were similar to those measured the previous summer, with a negative slope of —(25.1 μmol kg1 μmol kg<sup>-1</sup> per salinity unit, slightly above the mixing line, indicating TA production (Fig. 3a).). The DIC concentrations also showed a similar pattern during both summer cruises (Table 3; Fig. 3b)<sub>2</sub>, with negative slopes of - 49.0 μmol kg<sup>-1</sup> and - 44.3 μmol kg<sup>-1</sup> per salinity unit in July 2021 and 2022, respectively, in the Eastern WS (Table 3; Fig. 3a)<sub>2</sub>.

Table 3: Overview of different the parameters TA (μmol kg<sup>-1</sup>), DIC (μmol kg<sup>-1</sup>) and [TA-DIC] (μmol kg<sup>-1</sup>) of all seasonal samplings in average with the standard deviation.

Parameter	July 2021	October 2021	March 2022	May 2022	July 2022
TA (µmol					
$kg^{-1}$ )	$2403.4 \pm 27.4$	$2388.6 \pm 15.6$	$2358.6 \pm 27.8$	$\frac{2378.9}{2379} \pm 39.0$	$2380.2 \pm 42.7 \pm 43$
Western	$\frac{2283.5}{2284} \pm 10.2$	$2236.62389 \pm 16$	$2359 \pm 28$	$2349.7 \pm 9.8 2350 \pm 10$	$2337.2 \pm 35.2$
WS		$2237 \pm 5.3$	$2347.2 \pm 11.8 \pm 12$		
Eastern					
WS					
DIC (µmol					
$kg^{-1}$ )	$\frac{2185.8}{2186} \pm 48.2$	$2257.1 \pm 91.0$	$2237.7 \pm 37.8$	$\frac{2065.5}{2066} \pm 107.0$	$2184.4 \pm 43.3$
Western	$2124.1 \pm 10.3$	$\frac{2182.8}{2183} \pm 18.2$	$2211.8 \pm 20.9 \times 2238 \pm 38$	$2089.2 \pm 38.0$	$2142.3 \pm 27.6 \pm 28$
WS			$2212 \pm 21$		
Eastern					
WS					
[TA-DIC]					
(µmol kg <sup>-1</sup> )					
Western	$217.55 \pm 51.9$	$150.5 \pm 47.1$	$\frac{120.9}{121} \pm 30.2$	$313.3 \pm 76.1$	$196.8 \pm 26.7$
WS	$218 \pm 52$	$\underline{184.9 \pm 19.9} \underline{185 \pm 20}$	<del>137.9</del> - <u>138</u> ± 11 <del>.0</del>	$260.5 \pm 34.7261 \pm 35$	$\frac{194.9}{197 \pm 27}$
Eastern	$159.44 \pm 16.4$				$195 \pm 21.1$
WS					

In October 2021, the highest TA concentrations were measured TA peaked at a station near-Norddeich (up to 2571 umol kg<sup>-1</sup>) in the Western WS (up to 2571 µmol kg<sup>-1</sup>; Fig. 2). The DIC values reached a maximum of 2516 µmol kg<sup>-1</sup> in front of Norderney<sup>-1</sup> and decreased with increasing longitude eastward to a minimum of 2158 μmol kg<sup>-1</sup> (Fig. 2). The mixing plot of TA in October 2021 shows a negative. The TA mixing line in the Western WS (-had a negative slope (-25.4 \text{ \text{\mu}} mol kg<sup>-1</sup>-1 per salinity unit), whereas while the Eastern WS shows an almost showed a near-linear mixing line with a positive slope of (+13.1 310 μmol kg<sup>-1</sup> per salinity unit) (Fig. 3d). 2; Fig. DIC conservative mixing lines revealed a similar pattern, with a steep negative slope (-46.9 µmol kg<sup>-1</sup><del>2e). A similar picture of TA was observed in the Western WS (-46.9 mol kg<sup>-1</sup> per salinity unit) in the</del> Western WS (Fig. 3c). (Fig. This consistent difference across both parameters highlights strong spatial heterogeneity in carbonate system dynamics 3d). In March 2022, lower DIC concentrations (< 2200 µmol kg<sup>-1</sup>) were measured further offshore behind the islands of Borkum, Juist and Norderney, which increased slightly closer to land (Fig. 2). 315 The mean measured TA-Relatively low DIC values (<2200 µmol kg<sup>-1</sup> in the Western WS) were observed outside the barrier islands in March, with slight increase towards the coast (Fig. 2). During this season, TA concentrations showed little deviation from conservative mixing during this season. The mixing lines exhibited weak negative slopes in both subregions (-7.5 µmol kg<sup>-1</sup> per salinity unit in the Western WS and -6.8 μmol kg<sup>-1</sup> per salinity unit in the Eastern WS; Fig. 3f), indicating that TA 320 dynamics were largely controlled by physical mixing with only a minor signal of net production. Similarly, DIC mixing lines revealed shallow negative slopes (-18.2 and -15.9 µmol kg<sup>-1</sup> per salinity unit in the Western and Eastern WS, respectively; Fig. 3e). Mean TA values in the Western WS reached 2379 μmol kg<sup>-1</sup> in May was 2378.9 μmol kg<sup>+</sup> (Table 3<sub>τ</sub>; Fig. 2), indicating reflecting a slightmoderate seasonal increase in TA from March to May 2022. Most of the TA values were, with 325 concentrations generally close to or slightly above the mixing line, with and showing similar negative slopes in the Western (15.6 μmol kg<sup>-1</sup> per salinity unit) and in the Eastern WS (15.6 μmol kg<sup>-1</sup> per salinity unit) and Eastern WS (15.6 μmol kg<sup>-1</sup> per salinity unit) and Eastern WS (15.6 μmol kg<sup>-1</sup> per salinity unit) and Eastern WS (15.6 μmol kg<sup>-1</sup> per salinity unit) and Eastern WS (15.6 μmol kg<sup>-1</sup> per salinity unit) and Eastern WS (15.6 μmol kg<sup>-1</sup> per salinity unit) and Eastern WS (15.6 μmol kg<sup>-1</sup> per salinity unit) and Eastern WS (15.6 μmol kg<sup>-1</sup> per salinity unit) and Eastern WS (15.6 μmol kg<sup>-1</sup> per salinity unit) and Eastern WS (15.6 μmol kg<sup>-1</sup> per salinity unit) and Eastern WS (15.6 μmol kg<sup>-1</sup> per salinity unit) and Eastern WS (15.6 μmol kg<sup>-1</sup> per salinity unit) and Eastern WS (15.6 μmol kg<sup>-1</sup> per salinity unit) and Eastern WS (15.6 μmol kg<sup>-1</sup> per salinity unit) and Eastern WS (15.6 μmol kg<sup>-1</sup> per salinity unit) and Eastern WS (15.6 μmol kg<sup>-1</sup> per salinity unit) and Eastern WS (15.6 μmol kg<sup>-1</sup> per salinity unit) and Eastern WS (15.6 μmol kg<sup>-1</sup> per salinity unit) and Eastern WS (15.6 μmol kg<sup>-1</sup> per salinity unit) and Eastern WS (15.6 μmol kg<sup>-1</sup> per salinity unit) and Eastern WS (15.6 μmol kg<sup>-1</sup> per salinity unit) and Eastern WS (15.6 μmol kg<sup>-1</sup> per salinity unit) and Eastern WS (15.6 μmol kg<sup>-1</sup> per salinity unit) and Eastern WS (15.6 μmol kg<sup>-1</sup> per salinity unit) and Eastern WS (15.6 μmol kg<sup>-1</sup> per salinity unit) and Eastern WS (15.6 μmol kg<sup>-1</sup> per salinity unit) and Eastern WS (15.6 μmol kg<sup>-1</sup> per salinity unit) and Eastern WS (15.6 μmol kg<sup>-1</sup> per salinity unit) and Eastern WS (15.6 μmol kg<sup>-1</sup> per salinity unit) and Eastern WS (15.6 μmol kg<sup>-1</sup> per salinity unit) and Eastern WS (15.6 μmol kg<sup>-1</sup> per salinity unit) and Eastern WS (15.6 μmol kg<sup>-1</sup> per salinity unit) and Eastern WS (15.6 μmol kg<sup>-1</sup> per salinity unit) and Eastern WS (15.6 μmol kg<sup>-1</sup> per salinity unit) and Eastern WS (15.6 μmol kg<sup>-1</sup> per salinity unit) and Eastern WS (15.6 μmol kg<sup>-1</sup> per salinity unit) and Eastern WS (15.6 μmol kg<sup>-1</sup> per salinity unit) and Eastern WS (15.6 μmol kg<sup>-1</sup> per salinity unit) and Eastern WS (15.6 μmol kg<sup>+-1</sup> per salinity unit) (Fig. 3g). 3h). During this period, the signal of TA production was most clearly expressed in the Western WS. The lowest DIC values concentrations of the study (down to 1872 μmol kg<sup>-1</sup>) in this study (down to 1872 μmol kg<sup>-1</sup>) were also measured in the

Western WSobserved in spring (Table 3; Fig. 2; Fig. 3h 3g).



We note that conservative mixing lines in intertidal areas are often difficult to resolve visually, especially when data cluster closely. To better capture non-conservative variability, we calculated  $\Delta \text{DIC}_{\text{excess}}$  and  $\Delta \text{TA}_{\text{excess}}$  for each season and region, reflecting deviations from mixing. In addition,  $\Delta \text{TA}_{\text{P}}$  was derived as an upper estimate of photosynthetically driven TA changes. These metrics reduce uncertainty and provide a clearer assessment of net production and consumption than graphical mixing lines alone.

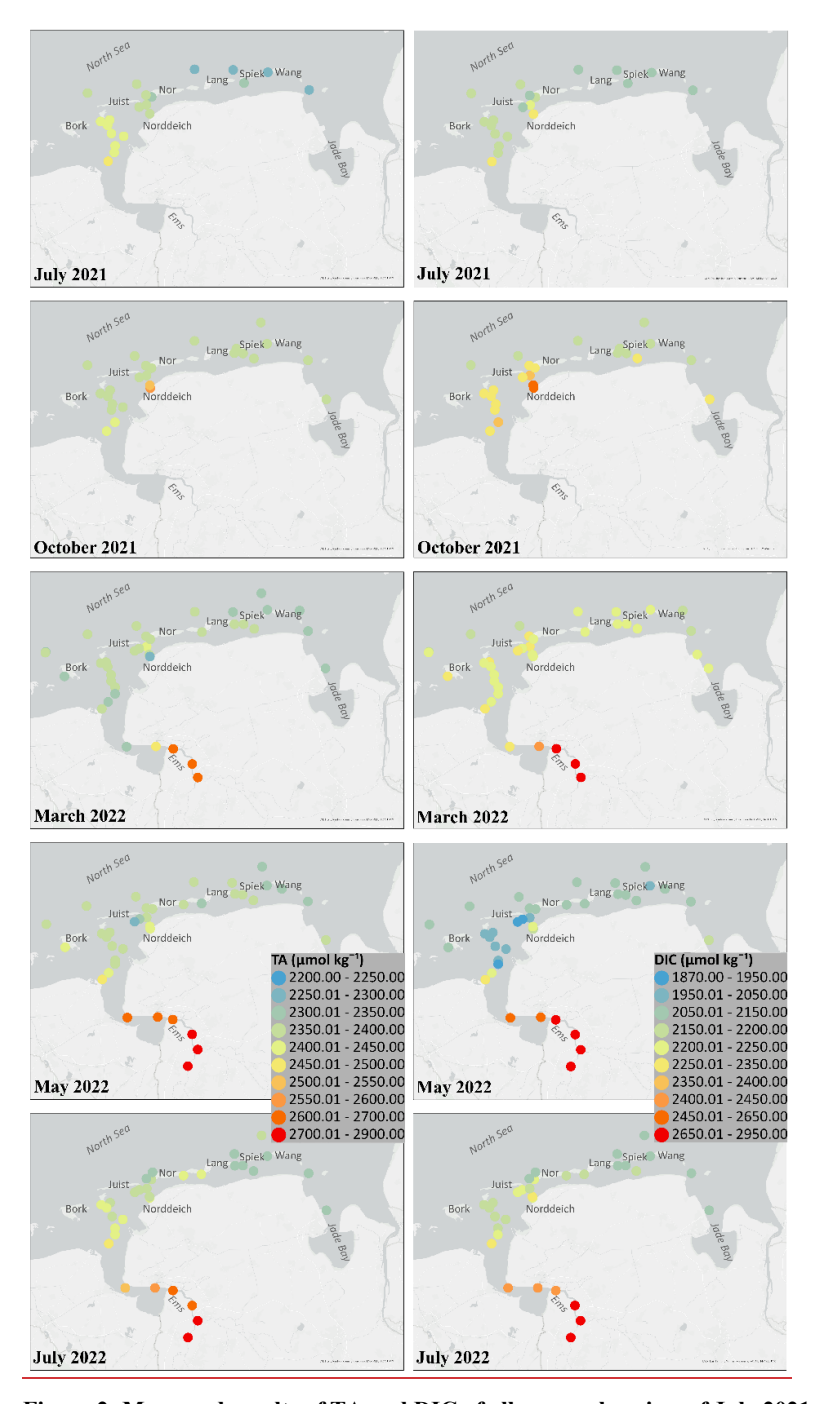


Figure 2: Measured results of TA and DIC of all seasonal cruises of July 2021, October 2021, March 2022, May 2022 and July 2022. All TA and DIC values are in  $\mu$ mol kg <sup>-1</sup>). The map in this Figure was generated using ArcGIS. Data sources: LGLN, Esri, TomTom, Garmin, Foursquare, FAO, METI/NASA, USGS. © 2024 Julia Meyer.

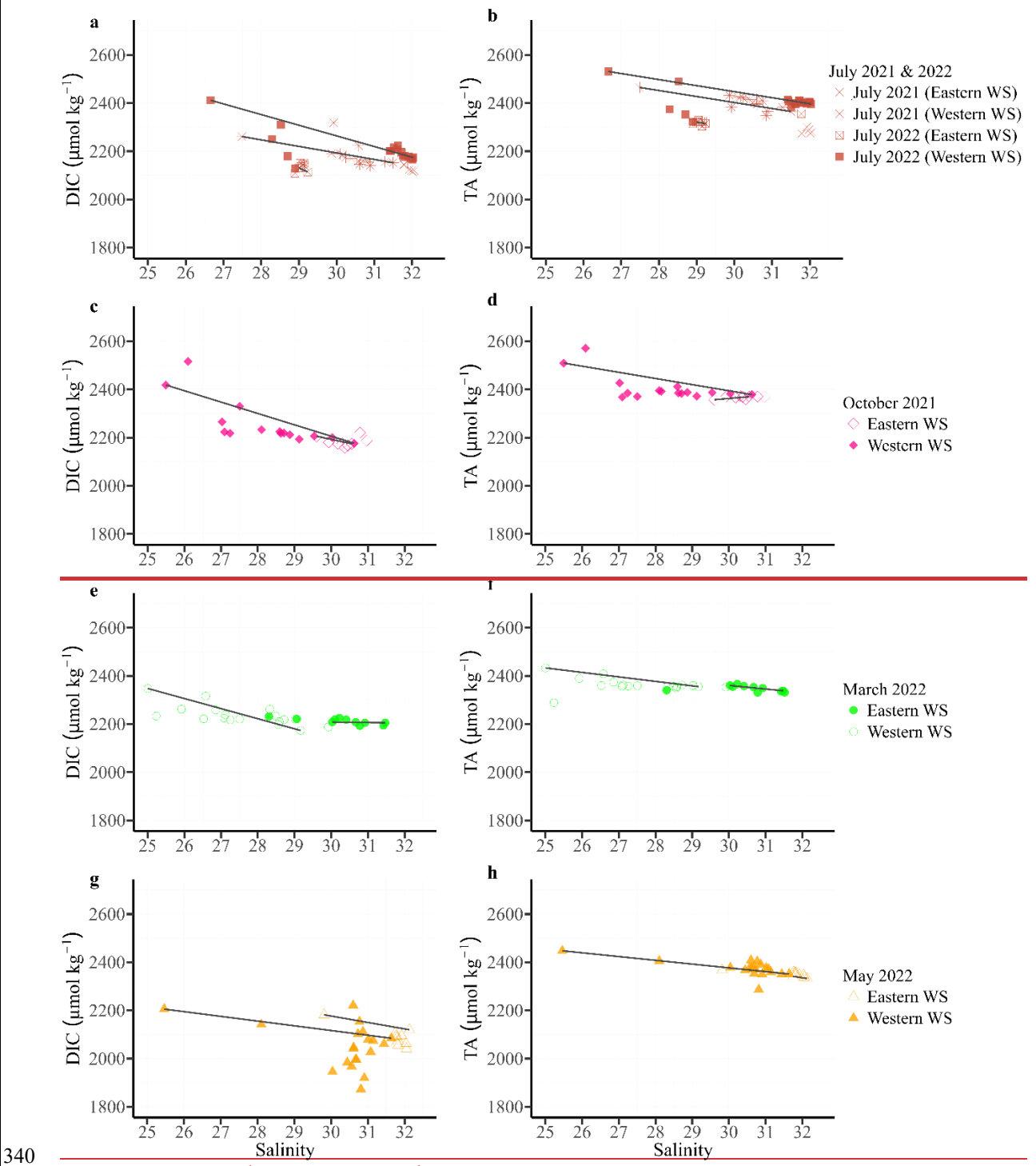


Figure 3: TA (µmol kg<sup>-1</sup>) and DIC (µmol kg<sup>-1</sup>) mixing plots, against salinity of July 2021 (a, b), October 2021 (c, d), March 2022 (e, f), May 2022 and July 2022 (a, b) at > 25 salinity, separated by the different regions (Eastern WS, Western WS) of the EFWS.



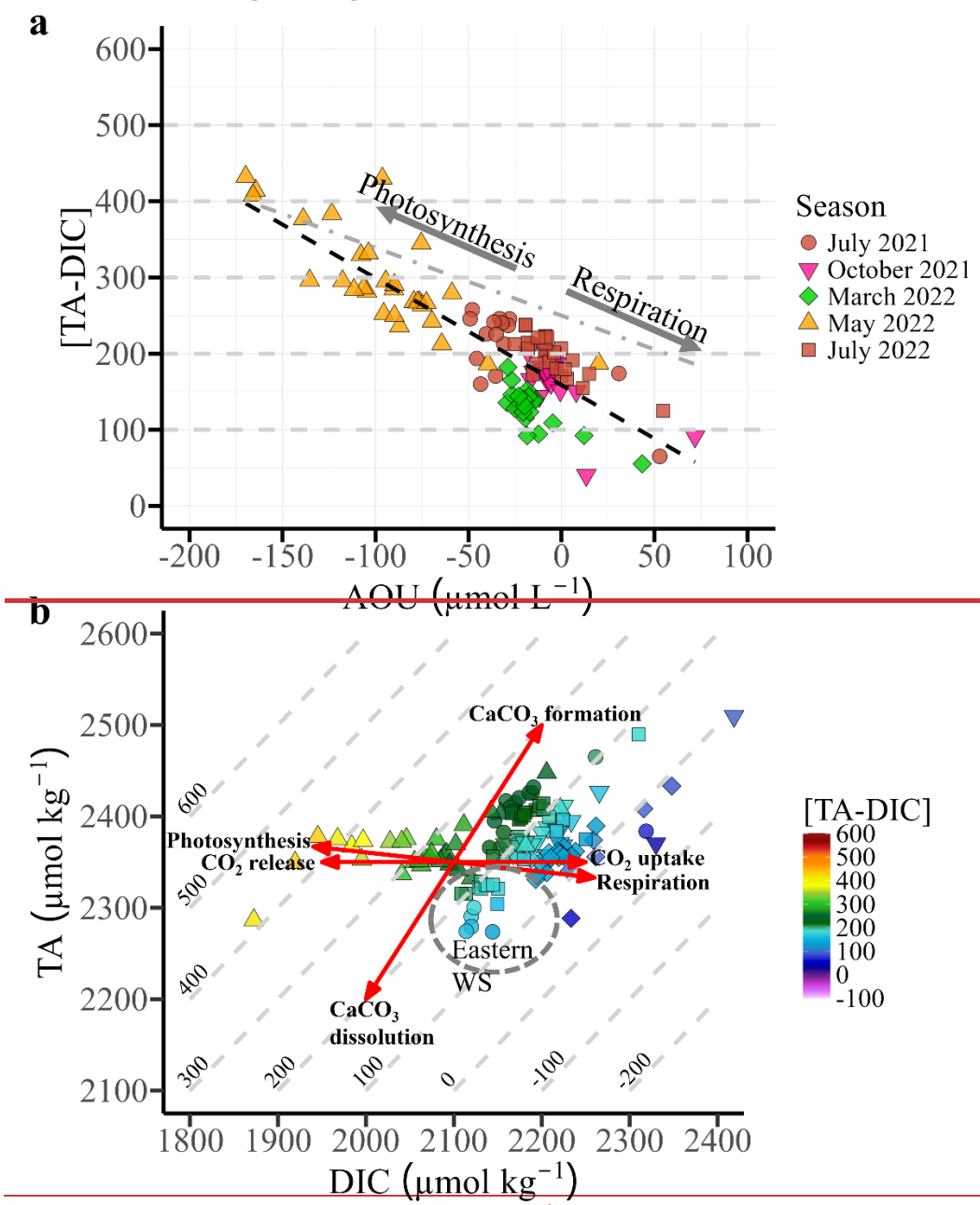


Figure 4: (a) AOU relationship to [TA DIC] in μmol kg<sup>-1</sup> of all seasonal cruises with the related regression analysis (black dashed line). The arrows show the possible processes that could affect the [TA DIC] and apparent oxygen utilization (AOU). The grey dashed line represents the regression line, which illustrates the Redfield ratio slope (-123/138 = -0.89), proposed by Xue & Cai (2020). (b) DIC versus TA plot from all seasons, with the coloured value of [TA DIC] in μmol kg<sup>-1</sup> of the EFWS with salinity 25-32.5. The isoclines are representing the [TA DIC] values. The red lines showing the related biogeochemical processes (Photosynthesis /Respiration, CO<sub>2</sub> release / uptake and CaCO<sub>3</sub> formation / dissolution). The Eastern part of the EFW is highlighted here with the grey cycle.

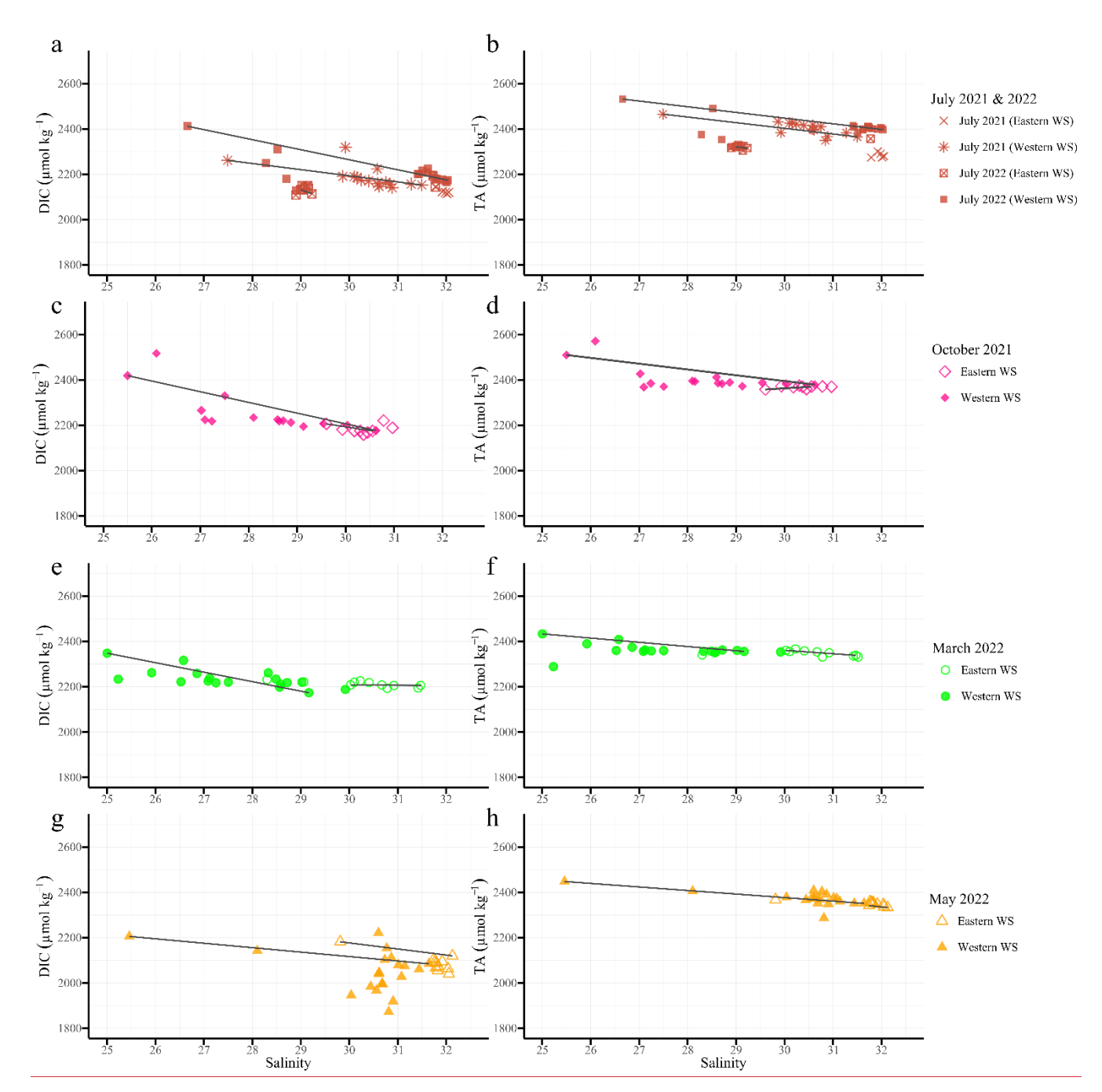


Figure 3: Conservative mixing plots of DIC (left column) and TA (right column) in μmol kg<sup>-1</sup> versus salinity in the EFWS, separated by cruise and region. Each plot includes data from both Eastern and Western regions (different symbols). Rows correspond to cruises: (a, b) July 2021 and July 2022, (c, d) October 2021, (e, f) March 2022, and (g, h) May 2022. Solid lines represent conservative mixing lines. Only data with salinity >25 are shown, illustrating seasonal and regional variability along the land-to-sea gradient in the EFWS.

## 3.3 Seasonal Dynamics of DIC and TA Excess and Primary Production Effects

370

375

380

Stations near Norddeich harbour, closer to the mainland, consistently exhibited the highest TA (up to 2571 μmol kg<sup>-1</sup> in October) and DIC (up to 2516 μmol kg<sup>-1</sup> in October) concentrations across all seasons (see section 3.2; Fig. 2). These locally high values were therefore excluded from the calculation of mean ± standard deviation to provide a more representative assessment of ΔDIC<sub>excess</sub>, ΔTA<sub>excess</sub>, and ΔTA<sub>P</sub>. However, these values are still displayed in the scatter plots (Fig. 4) to illustrate the range of variability, including highly positive and negative deviations.

365 Table 4: Mean  $\pm$  Standard Deviation of  $\triangle DIC_{excess}$ ,  $\triangle TA_{excess}$ , and  $\triangle TA_P$  (µmol kg<sup>-1</sup>) in the Eastern and Western EFWS of all seasons and regions. One-sample t-tests against zero (representing conservative mixing between North Sea and estuarine waters) were performed. Significant deviations from zero are indicated with symbols (\* p < 0.05, \*\* p < 0.01, \*\*\* p < 0.001).

Season	<u>July 2021</u>	October 2021	March 2022	<u>May 2022</u>	<u>July 2022</u>
<b><u>ADIC</u></b> excess					
Western WS:	23.4 ± 27.6 *	$47.7 \pm 84.9$	20.5 ± 23.8 **	-69.3 ± 107.0 *	54.6 ± 33.3 ***
Eastern WS:	$-19.3 \pm 11.2 *$	$-6.4 \pm 19.4$	$5.6 \pm 11.2$	-30.1 ± 35.8 *	$-16.0 \pm 26.2$
ΔTA <sub>excess</sub>					
Western WS:	123.0 ± 27.8 ***	$29.9 \pm 51.9$	$16.6 \pm 21.9$ **	36.6 ± 36.1 ***	$50.9 \pm 21.9$ ***
Eastern WS:	$10.9 \pm 11.5$	$-2.4 \pm 5.9$	10.7 ± 12.5 *	18.8 ± 13.8 ***	-34.7 ± 32.3 **
$\Delta TA_{P}$					
Western WS:	-3.6 ± 4.4 *	$-7.7 \pm 13.6$	-3.3 ± 3.8 **	11.1 ± 17.2 *	$-8.8 \pm 5.4$ ***
Eastern WS:	3.1 ± 1.8 *	$1.0 \pm 3.1$	$-0.85 \pm 1.7$	$4.8 \pm 5.7$ *	$2.6 \pm 4.2$

Seasonal deviations in  $\Delta DIC_{excess}$ ,  $\Delta TA_{excess}$ , and  $\Delta TA_P$  were evaluated using one-sample t-tests against a null hypothesis of zero for each Season and Region, where zero represents the scenario in which all DIC and TA at a station are solely the result of conservative mixing between North Sea and estuarine waters, with no additional contributions from estuarine processes or biological activity.

The Western WS generally exhibits positive  $\Delta \text{DIC}_{\text{excess}}$  values, with a peak in October 2021 (47.7 ± 84.9 µmol kg<sup>-1</sup>, p = 0.078) and summer (July 2021: 23.4 ± 27.6 µmol kg<sup>-1</sup>; July 2022: 54.6 ± 33.3 µmol kg<sup>-1</sup>, p < 0.001), suggesting an excess of DIC beyond the expected mixing (Fig. 4a). In contrast, during May,  $\Delta \text{DIC}_{\text{excess}}$  in the Western WS was negative (-69.3 ± 107.0 µmol kg<sup>-1</sup>, p = 0.014), suggesting significant DIC consumption, due to enhanced primary production during spring bloom conditions. Similarly, negative values were observed in the Eastern WS in May 2022 (-30.1 ± 35.8 µmol kg<sup>-1</sup>, p = 0.014) and July 2021 (-19.3 ± 11.2 µmol kg<sup>-1</sup>, p = 0.018) (Table 4; Fig. 4a).

 $\Delta TA_{excess}$  also exhibited seasonal and regional patterns: in the Western WS, high positive and significant deviations were observed in July 2021 (123.0 ± 27.8 µmol kg<sup>-1</sup>, p < 0.001) and July 2022 (50.9 µmol kg<sup>-1</sup>, p = 2.36 × 10<sup>-6</sup>), reflecting additional alkalinity sources. In the Eastern WS,  $\Delta TA_{excess}$  was negative in July 2022 (-34.7 µmol kg<sup>-1</sup>, p = 0.005), whereas July 2021 showed a slight, non-significant positive deviation (10.9 µmol kg<sup>-1</sup>, p = 0.102) (Fig. 4b).

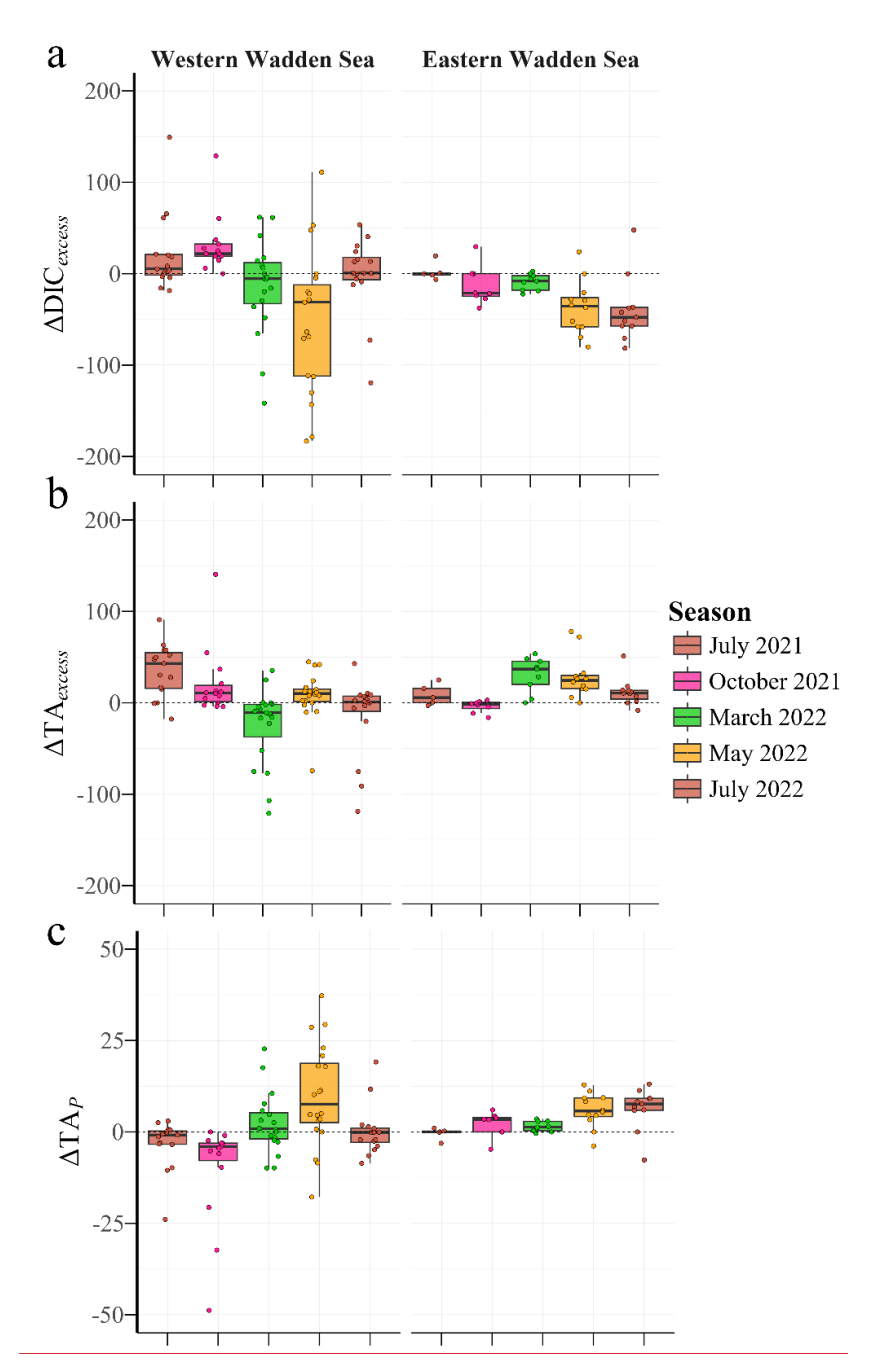


Figure 4: Boxplots of ΔDIC<sub>excess</sub>, (a) ΔTA<sub>excess</sub>, (b) and ΔTA<sub>P</sub> (c) in μmol kg<sup>-1</sup> in the Western WS (left panels) and Eastern WS (right panels) from each season. Each colour represents different seasons. Each box represents the interquartile range (IOR), with the median shown by the thick line.

 $\Delta TA_P$ , representing primary production effects, was positive in May in both the Western (11.1  $\mu$ mol kg<sup>-1</sup>, p = 0.014) and Eastern WS (4.83  $\mu$ mol kg<sup>-1</sup>, p = 0.014), indicating a significant impact on TA, during times with net uptake of CO<sub>2</sub> through

primary production with nitrate uptake, and a corresponding significant decrease in DIC (Fig. 4a, c). In other seasons, ΔTA<sub>P</sub> exhibited contrasting patterns between regions: ΔTA<sub>P</sub> in July in the Western WS was negative (July 2021: -3.8 μmol kg<sup>-1</sup>, 390 p = 0.010; July 2022: -8.75 μmol kg<sup>-1</sup>, p < 0.001), whereas in the Eastern WS ΔTA<sub>P</sub> was positive in July 2021 (3.1 μmol kg<sup>-1</sup>, p = 0.018), highlighting regional differences (Fig. 4c). To sum up, the Western WS exhibited higher and more variable deviations in ΔDIC<sub>excess</sub> and ΔTA<sub>excess</sub>, with significant summer TA production signal. In the Eastern WS, ΔDIC<sub>excess</sub> followed a similar seasonal pattern with smaller magnitudes, while ΔTA<sub>excess</sub> was positive in 2021 but turned significantly negative in July 2022. In the Eastern WS, ΔDIC<sub>excess</sub> followed a similar seasonal pattern with smaller magnitudes, while ΔTA<sub>excess</sub> was positive in 2021 but turned significantly negative in July 2022, which may indicate a stronger influence of sluice openings on TA.

#### 3.4 Influence of Biogeochemical Processes on Seasonal [TA-DIC] and AOU in the EFWS

400

The relationship between [TA–DIC] and AOU provides valuable insights into the biogeochemical processes that drive carbonate dynamics in coastal systems (Xue & Cai, 2020). A critical threshold for interpreting this relationship is that [TA–DIC] cannot be used when values are < 50 μmol kg<sup>-1</sup>, as proposed by Xue &and Cai (2020). This threshold applied only to one station near Norddeich harbor in October (Fig. 75), so these data were excluded from the seasonal calculations (Table 3).

Figure 4a5a illustrates the AOU relationship to [TA-DIC] from all stations sampled during various seasons in the Wadden Sea. The regression analysis highlights a negative correlation, with a slope of -1.41642  $\pm$  0.08 umol kg umol kg per umol Lumol L<sup>-1</sup> of AOU, which is steeper than the Redfield. When accounting for density-normalized O<sub>2</sub> (i.e., converting AOU 405 from  $\mu$ mol L<sup>-1</sup> to  $\mu$ mol kg<sup>-1</sup> using the potential density of seawater), the slope becomes  $-1.44 \pm 0.09 \,\mu$ mol kg<sup>-1</sup> per  $\mu$ mol kg<sup>-1</sup>. The grey dashed line in Fig. 5a represents the theoretical Redfield ratio slope (-123/138  $\approx$  -0.89), previously proposed by which Xue &and Cai (2020), summarize as a reference for expected [TA-DIC] changes per unit AOU in subsurface waters. In their framework, [TA-DIC] serves as a proxy for ocean acidification, directly linking biological production and respiration 410 to changes in DIC and TA. Biological production consumes CO<sub>2</sub> and nutrients, decreasing DIC and increasing TA, while respiration has the opposite effect, increasing DIC and decreasing TA; thus, the decomposition or formation of 1 mol of organic matter ((CH<sub>2</sub>O)<sub>106</sub>(NH<sub>3</sub>)<sub>16</sub>H<sub>3</sub>PO<sub>4</sub>) alters [TA–DIC] by ±123 mol, which can be approximated from the slope of ΔAOU. Deviations from the Redfield slope, for example in deep waters, may result from processes such as CaCO<sub>3</sub> dissolution, which increases both DIC and TA. Our measured slope in the Wadden Sea is steeper than the Redfield reference, indicating a stronger local biological influence on [TA-DIC]. 415

Based on the distribution of our dataset (Fig. 5), we use ~200 μmol kg<sup>-1</sup> [TA–DIC] as an empirical threshold that separates respiration-dominated conditions (lower [TA–DIC], positive AOU) from photosynthesis-dominated conditions with net TA production (higher [TA–DIC], negative AOU). We emphasize that this threshold is not a universal constant, but a pragmatic value derived from our dataset to interpret biogeochemical dynamics in the EFWS.

In spring, negative AOU values (down to -\_169 μmol L=1,-1; Fig. 4a) were observed alongside higher 5a) coincided with [TA-\_DIC] values (>-exceeding 200 μmol kg<sup>-1</sup>; Fig. 4b).

-1. In the summer (2021; 2022), [TA-DIC] values from the Eastern WS are located under the respiration/photosynthesis line (< 200 μmol kg<sup>-1</sup>; Fig. 4b5b). In contrast, the measured [TA-DIC] concentrations in the Western WS in summer are > 200 μmol kg<sup>-1</sup>, above the respiration/photosynthesis fit (Fig. 4b5b). In July 2022, the salinity in the same region changed by 2 - 3 units from one day (July 11) to another (July 12), where the salinity was higher in the East, showing. This short-term change in salinity is relevant to the observed TA and DIC because both parameters are partially controlled by conservative mixing, and slight increases in salinity can lead to proportionally higher TA values. Indeed, TA was slightly higher TA values in

#### 3.4 Seasonal Variability of DIC and TA in the EFWS: Influence of Mixing Processes

summer 2022 ( $+53.7 \pm \pm 36.7 \mu \text{mol kg}^{-1}$ ) in summer 2022, 1) compared to the previous year (Table 3).

430 Stations located near Norddeigh sharbour, closer eta the mainland, exhibit extreme values (Fig. 2) and therefore were

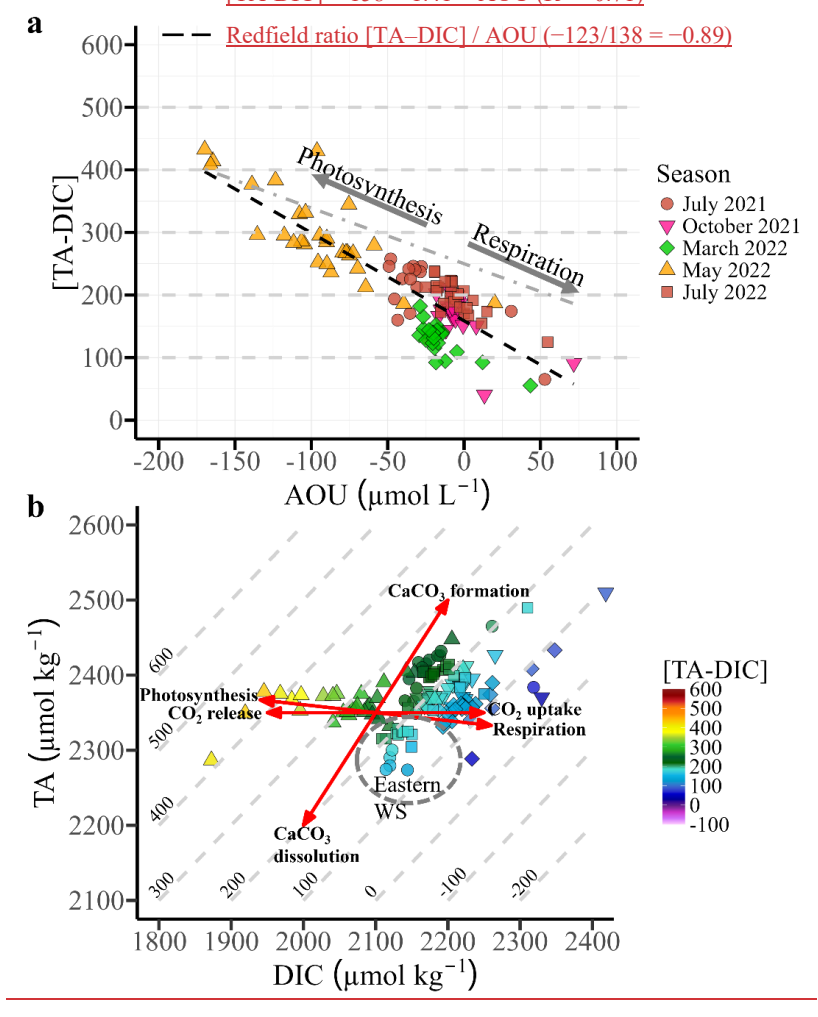


Figure 5: (a) AOU vs. [TA-DIC] (both in µmol kg<sup>-1</sup>) across all seasonal cruises, with regression analysis (black dashed line). Arrows indicate potential processes affecting [TA-DIC] and AOU. The grey dashed line represents the regression slope (- 123 / 138 = - 0.89) proposed by Xue and Cai (2020). (b) DIC versus TA plot from all seasons, with the coloured values of [TA-DIC] for the EFWS at salinity 25 – 32.5. Isoclines represent [TA-DIC] values. Red lines indicate key biogeochemical processes (photosynthesis / respiration, CO<sub>2</sub> exchange, and CaCO<sub>3</sub> formation / dissolution). The Eastern EFWS is highlighted with a grey circle.

excluded from the calculation of mean ± standard deviation to provide a more representative assessment of  $\Delta DIC_{excess}$ ,  $\Delta TA_{excess}$ , and  $\Delta TA_{P}$ . However, these values are still displayed in the scatter plots (Fig. 5) to illustrate the range of variability, including highly positive and negative deviations.

440 Table 4: Mean ± Standard Deviation of ADIC excess, ATA excess, and ATA μ (μmol kg<sup>-1</sup>) of all seasons in the Eastern and Western EFWS.

Season	<del>July 2021</del>	October 2021	March 2022	May 202	2 July 2022
ADIC					
ADIC excess					
Western WS:	$23.4 \pm 27.6$	$47.7 \pm 84.9$	$20.5 \pm 23.8$	$-69.3 \pm 107.0$	$54.6 \pm 33.3$
Eastern WS:	$-19.3 \pm 11.2$	$-6.37 \pm 19.4$	$5.85 \pm 11.2$	$-30.1 \pm 35.8$	$-16.0 \pm 26.2$
<b>ATA</b> excess					
Western WS:	$123.0 \pm 27.8$	$29.9 \pm 51.9$	$16.6 \pm 21.9$	$36.6 \pm 36.1$	$50.9 \pm 21.9$
Eastern WS:	$10.9 \pm 11.5$	$-2.35 \pm 5.87$	$10.7 \pm 12.5$	$18.8 \pm 13.8$	$-34.7 \pm 32.3$
<del>ATA</del> <sub>P</sub>					
Western WS:	$-3.75 \pm 4.43$	$\frac{-7.65 \pm 13.6}{}$	$-3.28 \pm 3.82$	$11.1 \pm 17.2$	$\frac{8.75 \pm 5.35}{}$
Eastern WS:	$3.10 \pm 1.80$	$1.02 \pm 3.11$	$-0.845 \pm 1.72$	$4.83 \pm 5.74$	$2.56 \pm 4.20$

435

445

450

2022 (54.6 ± 33.3 μmol kg<sup>-1</sup>), suggesting an excess of DIC beyond the expected mixing (Fig. 5a). In contrast, during May, ΔDIC<sub>excess</sub> in the Western WS was negative ( 69.3 ± 107.0 μmol kg<sup>-1</sup>), suggesting significant DIC consumption, potentially due to enhanced primary production during spring bloom conditions. Similarly, negative values were observed in the Eastern WS in May 2022 ( 30.1 ± 35.8 μmol kg<sup>-1</sup>) and July 2021 ( 19.3 ± 11.2 μmol kg<sup>-1</sup>) (Table 4; Fig. 5a). Higher ΔTΛ<sub>excess</sub> values are observed in the Western WS, particularly in July 2021 (123.0 ± 27.8 μmol kg<sup>-1</sup>), indicating additional alkalinity sources. In spring, ΔTΛ<sub>excess</sub> showed a clear positive trend, with an increase from March to May in both regions (Fig. 5b), suggesting that while TA is being consumed, production still exceeds consumption. The increases in TA from March to May were 20.0 ± 42.22 μmol kg<sup>-1</sup> in the Western WS and 8.1 ± 18.62 μmol kg<sup>-1</sup> in the Eastern WS (Table 4; Fig. 5). The Eastern WS exhibits lower ΔTΛ<sub>excess</sub> values, with some negative values in July 2022 ( 34.7 ± 32.3 μmol kg<sup>-1</sup>), when the sluice was open. ΔTΛ<sub>P</sub>, representing primary production effects, is positive in May (Table 4; Fig. 5c) in the Western and Eastern WS, indicating a net uptake of CO<sub>2</sub> through biological processes and a corresponding decrease in DIC (Fig. 5a).

The Western WS generally exhibits positive ΔDIC<sub>excess</sub> values, with a peak in October 2021 (47.7 ± 84.9 μmol kg<sup>-1</sup>) and July

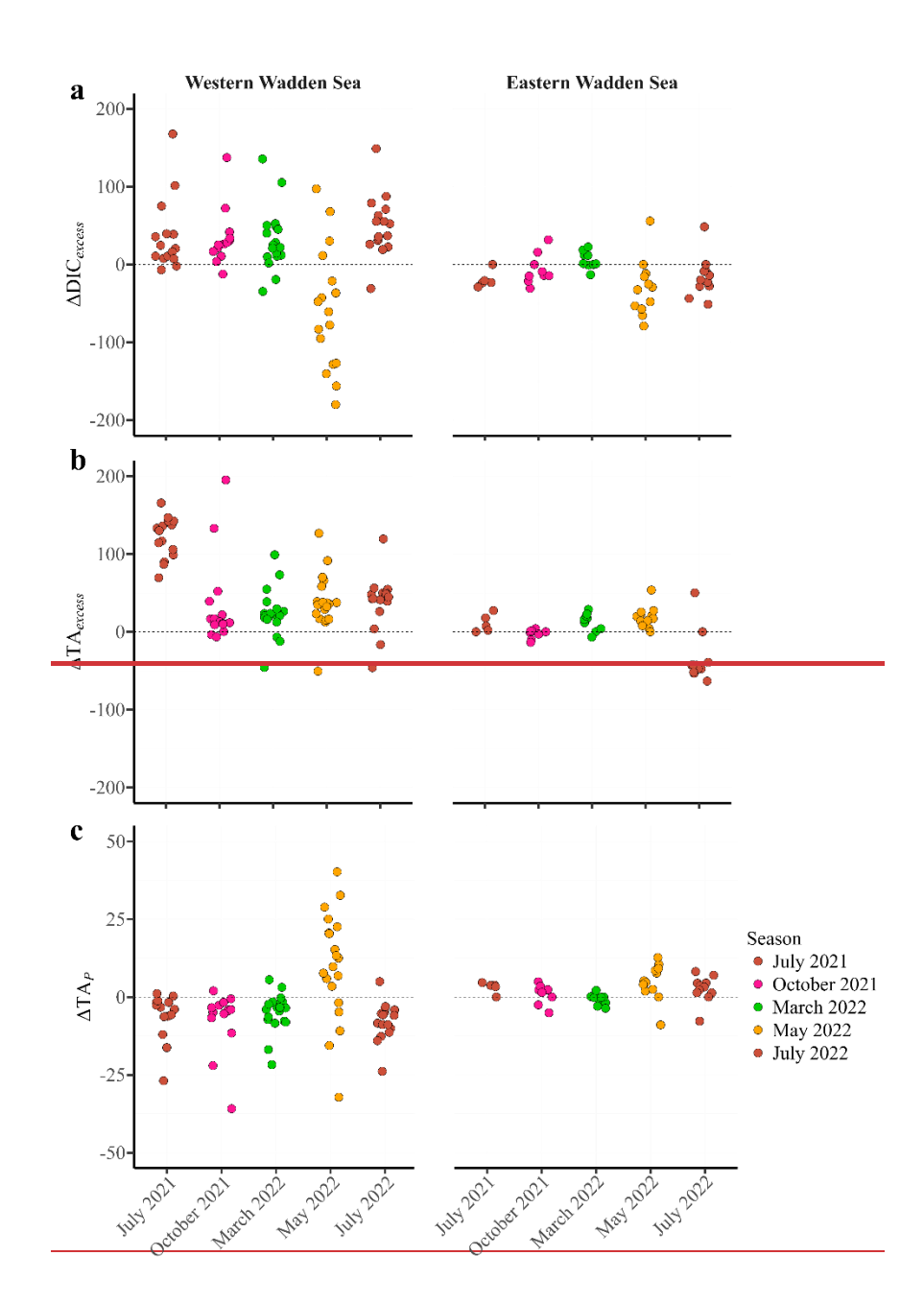
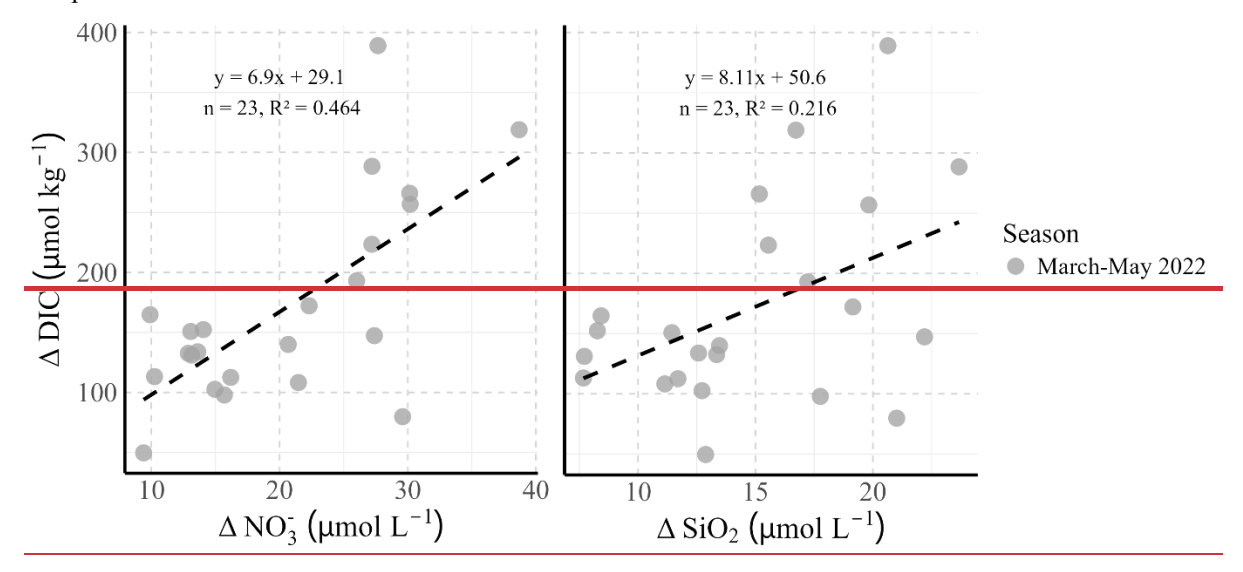


Figure 5: The scatter plots illustrate the seasonal variations of ADIC<sub>excess</sub>, (a) ATA<sub>excess</sub>, (b) and ATA<sub>P</sub> (c) in µmol kg<sup>-1</sup> in the Western WS (left panels) and Eastern WS (right panels) from each season. Each colour represents different seasons. 3.5 Regional and seasonal variation of Nutrients

A clear seasonal pattern can also be seen in the measured nutrients (Fig. S4). For NO<sub>2</sub><sup>-</sup> and NH<sub>4</sub><sup>+</sup> a decrease in concentrations was observed from October 2021 to May 2022, except in the East part of the EFWS (Fig. S4), where the concentration did not change much. NO<sub>3</sub><sup>-</sup> concentration ranged seasonally, with an increasing trend from summer to March 2022 (up to

460 66.28 μmol L<sup>-1</sup>) in the EFWS. In May 2022, the NO<sub>3</sub><sup>-</sup> concentrations decreased again below the detection limit of the instrument (> 0.01 μmol L<sup>-1</sup>) at some stations, mainly in the Western part (Fig. S4). This analogous seasonal tendency possibly will point to common sources and sinks.



465

470

475

Figure 6: NO<sub>3</sub>- and SiO<sub>2</sub> differences (ΔNO<sub>3</sub>-, ΔSiO<sub>2</sub>) of March to May 2022 against the difference of DIC (ΔDIC), with the related regression equations. The slopes show the Redfield Ratios of all measured stations in the Western and Eastern WS.

Overall, from March 2022 to May 2022 there was an average decrease in NO<sub>3</sub><sup>-</sup> of 19.29 ± 18.11 μmol kg<sup>-1</sup> (Fig. 6). TA slightly increased by 9.1 ± 29.2 μmol kg<sup>-1</sup> during this time (Fig. 4 - 6), while DIC decreased on average by 159.4 ± 125.4 μmol kg<sup>-1</sup>. The differences of NO<sub>3</sub><sup>-</sup> and SiO<sub>2</sub> for all stations between In figure 6, the changes from March and to May 2022 (ΔNO<sub>3</sub><sup>-</sup>, ΔSiO<sub>2</sub>) were (Δ May – March 2022) of NO<sub>3</sub><sup>-</sup> and SiO<sub>2</sub> at all stations are plotted against the corresponding change in DIC difference between March and May (ΔDIC, Fig. 6). For ΔNO<sub>3</sub><sup>-</sup>, a regression line was fitted with equation of y = 6.90x + 29.0891 (R<sup>2</sup> = 0.4637, 464, p value = < 0.05, Fig. 6), while the ΔSiO<sub>2</sub> regression has an equation of y = 8.11x + 50.6056 (R<sup>2</sup> = 0.2165216, p value = < 0.05; Fig. 6). The slopeslopes of both regression lines is these regressions represent the calculated C:N (6.90) and C:Si (8.11) ratios. Both values are close to the Redfield Ratio (Redfield 1963) ratios of 106½16—= 6.625 for NO<sub>3</sub><sup>-</sup> (6.90, Fig. 6(C:N)) and 106½15—= 7.067 for SiO<sub>2</sub> (8.11, Fig. 6), (C:Si) (Redfield et al., 1963), indicating that the identified enhanced primary production in this region in spring, along with nutrient (nitrate) and silicate uptake, most likely leadled to athe concomitant decrease in DIC (Fig. 6) and the observed increase in TA.

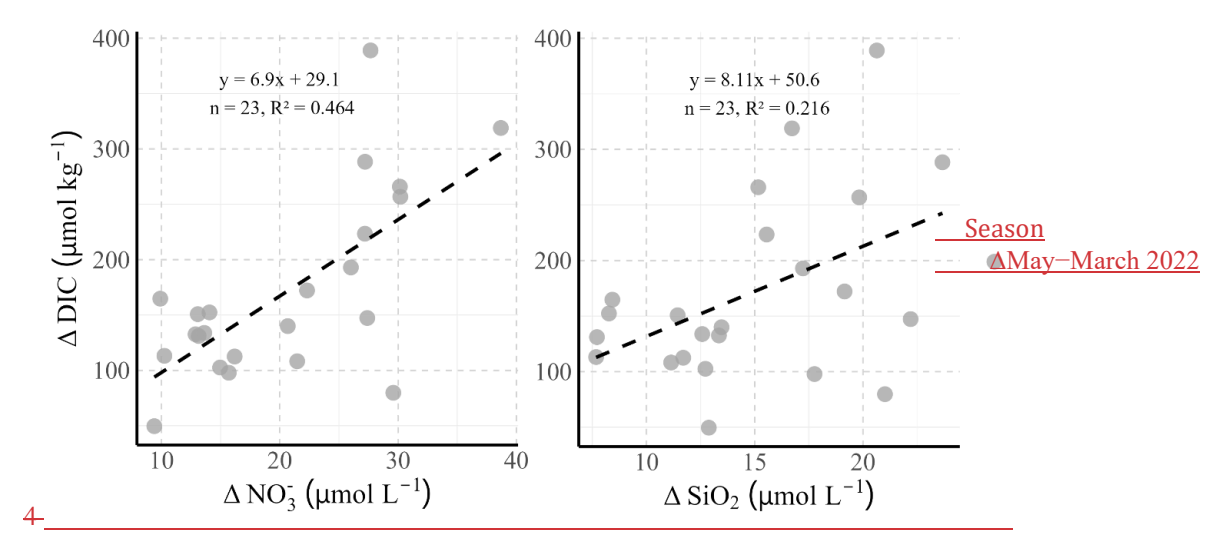


Figure 6: Differences between May and March 2022 for nitrate (ΔNO<sub>3</sub><sup>-</sup>) and silicic acid (ΔSiO<sub>2</sub>) plotted against the corresponding differences in DIC (ΔDIC) for all measured stations in the Western and Eastern Wadden Sea. Each point represents the change between the two months at a given station (Δ May – March 2022). Black dashed lines show linear regressions through the data, and the slopes correspond to the calculated C:N and C:Si ratios at the measured stations, derived from these differences.

## Discussion

480

485

490

## 4.1 Regional and seasonal Differences of the Carbonate Dynamics in the EFWS

This study highlights regional and seasonal variability in the carbonate system, with a notable West-to-East gradient in DIC and TA, showing considerable fluctuations across seasons (Table 3; Fig. 2). This is the first study to investigate ΔDIC<sub>excess</sub>, ΔTA<sub>excess</sub>, ΔTA<sub>P</sub> and [TA-DIC] in the EFWS to provide insights into the respective biogeochemical processes and to determine the source and sink dynamics of carbon on such a large spatial and temporal scale (Table 4; Fig. 54). We successfully demonstrated that TA increased in the spring because of intense primary production, most likely driven by nitrate uptake (Figs. 5Fig. 4; Fig. 6), highlighting the impact of biological activity on carbonate system dynamics. During the other seasons, the system acted as a source of DIC, indicating seasonal shifts in carbon cycling. Similar patterns of intense production periods and TA increases have also been reported in the North Sea adjacent to the Wadden Sea (Voynova et al., 2019). Additionally, we observed TA production during summer, which was more prominent in the Western WS, further suggesting that these intertidal regions act as a stronger source of TA and DIC during all seasons except in spring, compared to the Eastern EFWS.

# 4.2 Seasonal TA Production and DIC Dynamics in the EFWS

The data reveal important differences in the patterns between years and regions in summer (Table 4; Fig. 2 – 5). The observed summer dynamics in the Eastern and Western EFWS show distinct patterns in the biogeochemical processes related to TA and DIC production. Positive  $\Delta TA_{\text{excess}}$  (e.g.,  $123.0 \pm 27.8 \, \mu \text{mol kg}^{-1}$  in July 2021) and  $\Delta DIC_{\text{excess}}$  (23.4 ± 27.6; Table 4) values suggest that there is excessthe presence of additional sources of TA and DIC in the Western EFWSbeyond what would be

expected from conservative mixing between North Sea and estuarine waters. One key biogeochemical process, which can contribute to increasing TA, without a proportional increase in DIC, is the dissolution of CaCO<sub>3</sub>, which results in elevated [TA-DIC] values (>200 μmol kg<sup>-1</sup>) (Chen & Wang, 1999; Hoppema, 1990). However, CaCO<sub>3</sub> dissolution can be ruled out as a major TA source in the water column, since calcite is supersaturated (Ωcal > 1) during the study period (Brasse et al., 1999; Norbisrath et al., 2024). Nevertheless, in the sediments large amount of DIC can be produced by carbonate shells and transported by erosion processes into the water column (Brasse et al., 1999). Previous studies have estimated that TA production in the Wadden Sea is driven by anaerobic processes such as denitrification and/or CaCO<sub>3</sub> dissolution in sediments (Norbisrath et al., 2024; Thomas et al., 2009). Anaerobic degradation of organic matter—via denitrification and sulfate reduction—releases both TA and DIC (Brasse et al., 1999; Hu & Cai, 2011; Norbisrath et al., 2024; Thomas et al., 2009), with TA concentrations reaching up to 2310 μmol kg<sup>-1</sup> in summer (Thomas et al., 2009). Other studies suggest that permeable Janssand sediments (a tidal sand flat in the back-barrier area of Spiekeroog Island, Eastern EFWS) exhibit the highest potential denitrification rates (Gao et al., 2010).

In the summer months, the production of TA in both the Eastern and Western EFWS can be attributed to the decomposition of organic matter, especially following a productive spring season, such as the one observed in May 2022 (see section 4.3), which likely led to an elevated input of organic matter into the system (Borges et al., 2017). This organic matter subsequently undergoes both aerobic and anaerobic decomposition in the sediments during the summer months, where anaerobic processes like denitrification and sulphate reduction are drivers in generating both TA and DIC (Brasse et al., 1999; Norbisrath et al., 2024). These processes can significantly contribute to the enhancement of TA production (Fig. 4a,Fig. 4b; 5a, b; Fig. 5b), especially in the Western EFWS, where sedimentary anaerobic processes dominate in the summer (Al-Raei et al., 2009; Böttcher et al., 1998; Hu and& Cai, 2011; Kamyshny and& Ferdelman, 2010; Norbisrath et al., 2024; Thomas et al., 2009; Wu et al., 2015). Furthermore, with oxygen saturation remaining high (> 100 % saturation) and apparent oxygen utilization (AOU) being negative (Fig. 4a5a), it is evident that the water column is net autotrophic. This suggests that TA is primarily produced in the sediments and subsequently transported into the water column, rather than being generated in situ via remineralization (Beck & Brumsack, 2012; Postma, 1981).

Organic matter remineralization varies regionally across the North Frisian Wadden Sea (NFWS), EFWS, and Jade Bay (Kowalski et al., 2013; Van Beusekom et al., 2012). The NFWS favours aerobic degradation due to its wide tidal basins and high-water exchange (~8.1 km³ d⁻¹), resulting in lower organic matter accumulation, reduced eutrophication, and lower TA production relative to DIC ((Van Beusekom et al., 2012; Kowalski et al., 2013; Schwichtenberg et al., 2020); Van Beusekom et al., 2012). In contrast, the EFWS experiences higher eutrophication and organic matter accumulation due to its narrower basins and limited exchange, promoting anaerobic degradation processes (e.g., sulfate reduction), which enhance TA production (Kowalski et al., 2013; Schwichtenberg et al., 2020; Thomas et al., 2009; Van Beusekom et al., 2012). Jade Bay, with the lowest water exchange (~0.8 km³ d⁻¹), exhibits sporadic high TA/DIC ratios, likely due to short-term iron reduction processes (Brasse et al., 1999).).

A similar pattern was also seen in the Eastern EFWS compared to the Western in [TA-DIC] dynamics (Fig. \$12; Fig. 4b5b). In comparison to the Western, the Eastern EFWS consistently exhibits lower [TA-DIC] values (<200 μmol kg<sup>-1</sup>) during the summer months of 2021 and 2022, while the Western EFWS shows slightly higher [TA-DIC] values (>200 μmol kg<sup>-1</sup>; Fig. 4b5b). This difference can be attributed to enhanced CaCO3 formation, as indicated by its Ωcal (1.9 ± 0.8) in the Eastern (Fig. 4b). CaCO3 formation likely consumes TA (Chen, 1978), leading to the observed shift toward negative ΔTA<sub>excess</sub> values (Fig. 5b4b). The formation of CaCO3, particularly in sediments or shells, contributes to the lower observed source of TA in the Eastern compared to the Western WS. Despite this, the region still acts as a net source of TA, which aligns with the assumption that the Eastern EFWS can contribute TA to the coastal system during the summer months, especially from anaerobic degradation processes (Thomas et al., 2009; (Schwichtenberg et al<sub>7-12</sub> 2020; Thomas et al., 2009).).

Additionally, the salinity change observed in July 2022 was likely due to local anthropogenic influences, such as the sluice opening in summer 2022. On July 11, 2022, the sluice in Neuharlingersiel was opened just-before we started our sampling. This anthropogenic intervention likely caused sudden changes in salinity and local hydrological conditions (Fig. S1; Fig. 3a, b), making it reasonable to treat). Luebben et al. (2009) investigated the July 11 measurements influence of the sluice in the backbarrier area of Spiekeroog and found that the patterns of salinity, CDOM fluorescence, and DOC are strongly affected by the discharge of organic-rich freshwater via the sluice in Neuharlingersiel. Local freshwater inputs from sluices in the EFWS, such as anomalous. It is Neuharlingersiel—which can induce a salinity decrease of at least 1 unit (Luebben et al., 2009)—and potentially sluices in the Jade Bay (e.g. Dangaster Siel), as well as coastal circulation, may therefore play a more important to note that the role, although the exact contribution of each factor remains uncertain. While, the observed salinity drop extends beyond Norderney into Jade Bay, the low river discharge in summer (Pätsch & Lenhart, 2004; Schwichtenberg et al., 2020) suggests that large riverine inputs (e.g., from the Weser) are unlikely to be the primary cause. Importantly, lower [TA—DIC] values in the Eastern EFWS are were observed both on the day of sluice opening in July 2022 and on the day when the sluice was closed in July 2021. This suggests, suggesting that the impact of the sluice openingactivity did not have a major impact on the overall substantially control the [TA—DIC] dynamics in the region July 2022.

545

550

TheseThe seasonal shifts in TA can influence the coastal ocean's ability to absorb carbon from the atmosphere (Burt et al., 2016; Gruber et al., 2019; Li et al., 2024; Schwichtenberg et al., 2020). In summer, the generation of TA and DIC may alter the region's buffering capacity, with the Western WS possibly storing or taking up carbon (Fig. 7)-2; Fig. 3-5) (Gruber et al., 2019; Li et al., 2024). These findings align with previous studies (Thomas et al., 2009; Voynova et al., 2019) suggesting that the intertidal regions of the EFWS act as a source of both TA and DIC to the coastal system during the summer months.

Particularly, the tidal WS plays an important role in the biogeochemical cycling of the North Sea (Santos et al., 2015; Thomas et al., 2009), because many European rivers <u>are</u> empty in the WS (Thomas et al., 2009). A few studies discussed the generation in of TA in summer before (Schwichtenberg, 2013; Voynova et al., 2019) and the contribution of rivers (Pätsch and Lenhard, 2004). however in summer the riverine inflow iswas lowest, which could not explain an increase of TA in the WS. The highest riverine contribution of TA is expected from January to April (Pätsch & Lenhart, 2004; Schwichtenberg, 2013); Schwichtenberg et al., 2020).

.—The moderate rainfall and cooler-than-average weather in October 2021 may have influenced the hydrology of the region, potentially causing increased terrestrial runoff and enhanced delivery of alkalinity-rich water to the coastal system. The slight source of DIC in October (Table 3; Fig. 4d3c) suggests that organic matter remineralization and sediment-water exchange continue to play a role during this period (Borges et al., 2017). In addition, pore waters enriched with remineralized nutrients are actively released into the overlying water column (Beck & Brumsack, 2012) and organic matter-enriched water masses transported from the North Sea contribute to the availability of degradable material in the Wadden Sea, sustaining biogeochemical activity into autumn(Van Beusekom et al., 1999). This mechanism aligns with studies highlighting the importance of tidaltidally-driven nutrient and carbon fluxes in permeable sediments (Postma, 1981). transport processes facilitate the continuous exchange of dissolved carbon species between sediments and the water column (Santos et al., 2015). (Santos et al., 2015). Model simulations suggest that effective riverine inputs account for only about 5% of the total TA variability in the German Bight, implying that other processes—particularly tidal pumping—likely play a key role in sustaining elevated TA and DIC concentrations (Moore et al., 2011), as observed in October. In the Dutch Wadden Sea, De Groot et al. (2023) showed that tides control methanotrophic activity, which increases by ~40 % at low tide compared to high tide. By analogy, tidal cycles in the EFWS likely enhance advective transport of dissolved carbon from sediments to the water column, with Ra, TA, and DOC peaking at low tide and potentially driving substantial export to the adjacent North Sea (Moore et al., 2011), reinforcing the role of sediments as an active source of carbon and nutrients, consistent with the observations in October 2021.

## 4.3 Nitrate Assimilation and Carbonate Dynamics in Spring

570

580

The highest rates of photosynthesis were measured in our study in the spring of 2022 (May 2022). This is evidenced by high O<sub>2</sub> levels (up to 180 % saturation), low *p*CO<sub>2 obs</sub> (Table 2) and high chlorophyll a levels, along with negative AOU values (down to - 169 μmol L<sup>-1</sup>; Fig. 4a5a) (Artioli et al., 2012; Thomas et al., 2005b)2005). These findings highlight the dominant role of photosynthetic activity in modulating the carbonate system, particularly in the Western EFWS, where carbon fixation via photosynthesis is a key factor in this study. The resulting changes in [TA-DIC] during this period are reflected in the AOU to [TA-DIC] relationship shown in Figure 4a, with a steeper negative slope of -1.416 μmol kg<sup>-1</sup> per μmol L<sup>-1</sup> AOU, deviating from the Redfield ratio of -0.89 (Xue & Cai, 2020). This deviation suggests that the EFWS may differ from the typical conditions assumed in the Redfield model (Redfield et al., 1963), which is primarily based on aerobic respiration and production (Xue & Cai, 2020).

Furthermore, [TA-DIC] increased due to the significant decrease in DIC in May 2022 (Fig. 4b3c). Together with the positive  $\Delta$ TA<sub>P</sub> and strongly negative  $\Delta$ DIC<sub>excess</sub> values after removal of mixing, this supports the findings of intense spring primary production generating TA, while drawing down DIC (Fig. 54). This was particularly evident in the Western EFWS, but also in the Eastern, indicating the Western EFWS is a stronger sink for CO<sub>2</sub> due to carbon fixation and nitrate assimilation (Borges et al., 2005). The May measurements follow roughly the photosynthesis/respiration line, indicated by the progressively low DIC values in both regions, and slight increase in TA (9.1 ± 29.2  $\mu$ mol kg<sup>-1</sup> from March 2022 to May 2022; Fig. 4b5b), above

the mixing line (Fig. 3b3h). The relationship in Figure 6 also indicates that primary production is influenced by nitrate and silicate availability. Nitrate concentrations decreased substantially from 65  $\mu$ mol kg<sup>-1</sup> in March to 22  $\mu$ mol kg<sup>-1</sup> in May 2022 (Fig. 6; Fig. S4), coinciding with the period of intense primary production. This significant drawdown in nitrate concentrations suggests that nitrate assimilation was the primary driver of the observed decrease in DIC and the slight increase in TA during this period. Nitrate assimilation involves the consumption of hydrogen ions (H<sup>+</sup>) and the release of hydroxide ions (OH<sup>-</sup>), which leads to an increase in pH and, consequently, in TA (Brenner et al., 2016; Wolf-Gladrow et al., 2007). Therefore, nitrate assimilation played a crucial role in shaping the carbonate system dynamics by decreasing CO<sub>2</sub> and DIC, while increasing TA. The regression analysis of  $\Delta$ NO<sub>3</sub><sup>-</sup> and  $\Delta$ DIC between March and May 2022 revealed a slope of 6.90 for the changes in nitrate concentrations (Fig. 6), which is close to the Redfield ratio of 6.625 for the C:N ratio (Redfield; et al., 1963).) This close match suggests nitrate assimilation during the spring bloom, which is closely linked to a reduction in DIC. Similarly, the  $\Delta$ SiO<sub>2</sub> regression produced a slope of 8.11 (Fig. 6), which is also close to the Redfield ratio for SiO<sub>2</sub> (7.067), further supporting the conclusion that the enhanced primary production in this region during the spring bloom contributed to nutrient uptake, particularly nitrate and silicate.

We therefore propose that assimilation of  $NO_3^-$  during the time of intense primary production in May 2022 could explain the local increase of total alkalinity during the spring bloom. First, the maximum concentration of  $NO_3^-$  was captured in March before the high biologically productive season started in May 2022 (Fig. 4-73-6

615 ), with maximum concentrations measured in the Western WS. A significant drawdown of NO<sub>3</sub><sup>-</sup> from the maximum value of 65 μmol kg<sup>-1</sup> in March 2022 to 22 μmol kg<sup>-1</sup> in May 2022, resulted in an average decrease of 19.2 ± 9.6 μmol kg<sup>-1</sup> of NO<sub>3</sub><sup>-</sup> (Fig. 6; Fig. S4). Brewer &and Goldman (1976) also documented that nitrate assimilation increases TA (9.1 ± 29.2 μmol kg<sup>-1</sup>).

An uptake of NH<sub>4</sub><sup>+</sup> was not obvious, because NH<sub>4</sub><sup>+</sup> concentrations were much lower during this period (Fig. S4), suggesting only a small impact on TA patterns. Therefore, the limited influence of NH<sub>4</sub><sup>+</sup> uptake This further emphasizes the central role of nitrate assimilation via primary production in shaping the observed patterns in the carbonate system in the spring-early summer, and the role of land-based nitrate inputs to the coast. Nitrification, the process by which NH<sub>4</sub><sup>+</sup> is converted into NO<sub>2</sub><sup>-</sup>, causes a decrease in TA by 2 moles per mole of nitrogen (Wolf-Gladrow et al., 2007; Xue & Cai, 2020), thus has the opposite effect compared to nitrate assimilation, which increases TA. The decrease in NO<sub>3</sub><sup>-</sup> from May to July 2022 was less pronounced (1.51 ± 5.16 μmol kg<sup>-1</sup>, Fig. 6), which is consistent with the general trend of lower NO<sub>3</sub><sup>-</sup> concentrations in summer, likely driven by higher turnover rates (Kieskamp et al., 1991).

#### 5 Conclusions Conclusion

600

605

610

620

625

630

The findings highlight significant regional and seasonal variations in the EFWS carbonate system, reflecting broader carbon dynamics in coastal and shelf seas. Both TA and DIC exhibit substantial variations across regions and seasons, with a notable decrease in DIC from East to West and an increase in TA during biologically productive periods, such as spring and summer.

In spring 2022, a significant drawdown of NO<sub>3</sub> was observed, correlating with a slight increase in TA, likely due to nitrate assimilation during primary production. Primary production could explain up to 88 % of the \DIC<sub>excess</sub> in the Western WS and up to 92 % in the Eastern WS, contributing to the significant drop in DIC, slight TA production, and NO<sub>3</sub><sup>-</sup> drawdown during this period.

In the summer, it is likely that the remineralization of organic matter, combined with the dissolution of CaCO₃ in sediments, contributes to higher TA production, especially in the coastal and nearshore areas of the Western EFWS. On the other hand, our work suggested possible CaCO<sub>3</sub> formation in the Eastern EFWS may experience greater CaCO<sub>3</sub> formation, which may reduce TA levels ([TA-DIC] < 200 μmol kg<sup>-1</sup>). However, the region still acts as a net source of TA, in part due to the known high rates of benthic anaerobic respiration, such as organic matter decomposition and associated TA production, particularly after the high productivity of the spring season. This TA generation may enhance the region's capacity to absorb CO<sub>2</sub>, despite the broader southern North Sea generally being considered a carbon source to the atmosphere. These findings emphasize the complexity of the biogeochemical processes driving regional and seasonal variability in the EFWS carbonate system. particularly those influenced by tidal cycles, river inputs, and sediment interactions. Riverine inputs, especially from the Ems River estuary, also influence local carbonate chemistry. However, the relatively low river inflows during the summer suggest that sediment processes, such as organic matter decomposition, may play a more dominant role.

To gain a comprehensive understanding of these intricate interactions and their impact on carbon storage and marine biogeochemistry in this ecologically important region, further research, including sediment studies and continuous tidal monitoring, is essential. This study is the first to combine the analysis of [TA-DIC] with other parameters such as  $\Delta TA_{\text{excess}}$ ,  $\Delta DIC_{excess}$ , and  $\Delta TA_P$  to infer underlying biogeochemical processes - such as biological productivity and nutrient availability. This innovative approach offers a new way to examine how various environmental factors interact and influence the carbonate system. The results have the potential to refine existing models of the biogeochemical cycle, providing valuable insights for more accurate climate predictions and improved strategies for managing coastal systems in response to environmental change.

#### Code and data availability

635

640

650

655

The data supporting our findings withinin this study have been submitted by Lara Luitjens (NLWKN) to the PANGAEA data repository and are currently undergoing final editorial processing. A DOI for the dataset will be available upon completion of the review process (Luitjens et al., in review). The datasets can be accessed through the following links: https://doi.pangaea.de/10.1594/PANGAEA.974424

https://doi.pangaea.de/10.1594/PANGAEA.974426

https://doi.pangaea.de/10.1594/PANGAEA.974427

660 https://doi.pangaea.de/10.1594/PANGAEA.974428

## **Competing interests**

The contact author has declared that none of the authors has any competing interests.

## Acknowledgements

665

670

680

685

We thank Martina Gehrung, Tanja Pieplow, and Catharina Petrauskas for their exceptional technical support, meticulous work, and dedication. They ensured the reliability and accuracy of our data through their careful handling of samples and precise analytical measurements. We also thank Dr. Vlad-Alexandru Macovei for his assistance with processing the raw data from the pCO<sub>2</sub> sensor.

The scientists and crew who participated in the research expeditions, including the captain Alexander Heidenreich and the crew of the *RV Burchana* (Jens Voß and Winfried Bruns) are also greatly appreciated. It was their hard work, professionalism and co-operation during the challenging field work that made it possible to collect the data required for this study. The success of our research would not have been possible without your tireless efforts at sea. We thank all of you for your unwavering support and commitment.

Finally, we would like to acknowledge the support and valuable discussions with the members of the "CARBOSTORE" project and especially Prof. Dr. habil. Michael Böttcher from the Institute for Baltic Sea Research in Warnemünde (Germany).

The author wishes to express their gratitude to the anonymous reviewer for their constructive comments and valuable feedback, which significantly enhanced the manuscript.

## Financial support

This research was funded through the "CARBOSTORE" project (Grant Number 03F0875A), by the German Federal Ministry of Education and Research (BMBF). Additionally, the Helmholtz-Zentrum Hereon covered the article processing charges for this open-access publication.

## References

4H - Jena engineering GmbH. (2021). Data Processing for CONTROS HydroC ® CO2 (Manual). www.4h-jena.de

Al-Raei, A. M., Bosselmann, K., Böttcher, M. E., Hespenheide, B., & Tauber, F. (2009). Seasonal dynamics of microbial sulfate reduction in temperate intertidal surface sediments: controls by temperature and organic matter. *Ocean Dynamics*, 59(2), 351–370. https://doi.org/10.1007/s10236-009-0186-5

Artioli, Y., Blackford, J. C., Butenschön, M., Holt, J. T., Wakelin, S. L., Thomas, H., Borges, A. V., & Allen, J. I. (2012). The carbonate system in the North Sea: Sensitivity and model validation. *Journal of Marine Systems*, 102–104, 1–13. https://doi.org/10.1016/j.jmarsys.2012.04.006

- Bauer, J. E., Cai, W. J., Raymond, P. A., Bianchi, T. S., Hopkinson, C. S., & Regnier, P. A. G. (2013). The changing carbon cycle of the coastal ocean. In *Nature* (Vol. 504, Issue 7478, pp. 61–70). https://doi.org/10.1038/nature12857
  - Beck, M., & Brumsack, H. J. (2012). Biogeochemical cycles in sediment and water column of the Wadden Sea: The example Spiekeroog Island in a regional context. *Ocean and Coastal Management*, 68, 102–113. https://doi.org/10.1016/j.ocecoaman.2012.05.026
- Beck, M., Dellwig, O., Fischer, S., Schnetger, B., & Brumsack, H.-J. (2012). Trace metal geochemistry of organic carbon-rich

  watercourses draining the NW German coast. Estuarine, Coastal and Shelf Science, 104–105, 66–79.

  https://doi.org/10.1016/j.ecss.2012.03.025
  - Borges, A. V., Schiettecatte, L.-S., Abril, G., Delille, B., & Gazeau, F. (2006). Carbon dioxide in European coastal waters.

    Estuarine, Coastal and Shelf Science, 70(3), 375–387. https://doi.org/10.1016/j.ecss.2006.05.046
- Borges, A. V., Speeckaert, G., Champenois, W., Scranton, M. I., & Gypens, N. (2017). Productivity and Temperature as

  Drivers of Seasonal and Spatial Variations of Dissolved Methane in the Southern Bight of the North Sea. *Ecosystems*,

  21(4), 583–599. https://doi.org/10.1007/s10021-017-0171-7
  - Böttcher, M. E., Oelschläger, B., Höpner, T., Brumsack, H. J., & Rullkötter, J. (1998a1998). Sulfate reduction related to the early diagenetic degradation of organic matter and "black spot" formation in tidal sandflats of the German Wadden Sea (southern North Sea): Stable isotope (13C, 34S, 18O) and other geochemical results. *Organic Geochemistry*, 29(5-7–7 pt 2), 1517–1530. https://doi.org/10.1016/S0146-6380(98)00124-7
- Böttcher, M. E., Oelschläger, B., Höpner, T., Brumsack, H. J., & Rullkötter, J. (1998b). Sulfate reduction related to the early diagenetic degradation of organic matter and "black spot" formation in tidal sandflats of the German Wadden Sea (southern North Sea): stable isotope (13C, 34S, 18O) and other geochemical results. *Organic Geochemistry*, 29(5-7), 1517–1530. https://doi.org/10.1016/S0146-6380(98)00124-7

- Prasse, S., Reimer, A., Seifert, R., & Michaelis, W. (1999). The influence of intertidal mudflats on the dissolved inorganic carbon and total alkalinity distribution in the German Bight, southeastern North Sea. In *Journal of Sea Research* (Vol. 42).
  - Brenner, H., Braeckman, U., Le Guitton, M., & Meysman, F. J. R. (2016). The impact of sedimentary alkalinity release on the water column CO2 system in the North Sea. *Biogeosciences*, 13(3), 841–863. https://doi.org/10.5194/bg-13-841-2016
- Prewer, P. G., & Goldman, J. C. (1976). Alkalinity changes generated by phytoplankton growth1. *Limnology and Oceanography*, 21(1), 108–117. https://doi.org/10.4319/lo.1976.21.1.0108
  - Burt, W. J., Thomas, H., Hagens, M., Pätsch, J., Clargo, N. M., Salt, L. A., Winde, V., & Böttcher, M. E. (2016). Carbon sources in the North Sea evaluated by means of radium and stable carbon isotope tracers. *Limnology and Oceanography*, 61(2), 666–683. https://doi.org/10.1002/lno.10243
- 720 Chen, C. A., & Wang, S. (1999). Carbon, alkalinity and nutrient budgets on the East China Sea continental shelf. *Journal of Geophysical Research: Oceans*, 104(C9), 20675–20686. https://doi.org/10.1029/1999JC900055

- Chen, C.-T. A. (1978). Decomposition of Calcium Carbonate and Organic Carbon in the Deep Oceans. *Science*, 201(4357), 735–736. https://doi.org/10.1126/science.201.4357.735
- De Groot, T. R., Mol, A. M., Mesdag, K., Ramond, P., Ndhlovu, R., Engelmann, J. C., Röckmann, T., & Niemann, H. (2023).

  Diel and seasonal methane dynamics in the shallow and turbulent Wadden Sea. *Biogeosciences*, 20(18), 3857–3872. https://doi.org/10.5194/bg-20-3857-2023
  - Dickson, A. G. (1981). An exact definition of total alkalinity and a procedure for the estimation of alkalinity and total inorganic carbon from titration data. *Deep Sea Research Part A. Oceanographic Research Papers*, 28(6), 609–623. https://doi.org/10.1016/0198-0149(81)90121-7
- Dickson, A. G. (1990). Standard potential of the reaction: , and and the standard acidity constant of the ion HSO4- in synthetic sea water from 273.15 to 318.15 K. *The Journal of Chemical Thermodynamics*, 22(2), 113–127. https://doi.org/10.1016/0021-9614(90)90074-Z

- Duan, L., Song, J., Li, X., Yuan, H., & Zhuang, W. (2023). Potential risks of CO2 removal project based on carbonate pump to marine ecosystem. In *Science of the Total Environment* (Vol. 862). Elsevier B.V. https://doi.org/10.1016/j.scitotenv.2022.160728
- Feely, R., Doney, S., & Cooley, S. (2009). Ocean Acidification: Present Conditions and Future Changes in a High-CO2 World. *Oceanography*, 22(4), 36–47. https://doi.org/10.5670/oceanog.2009.95
- Friedlingstein, P., O'Sullivan, M., Jones, M. W., Andrew, R. M., Bakker, D. C. E., Hauck, J., Landschützer, P., Le Quéré, C.,
  Luijkx, I. T., Peters, G. P., Peters, W., Pongratz, J., Schwingshackl, C., Sitch, S., Canadell, J. G., Ciais, P., Jackson, R.
  B., Alin, S. R., Anthoni, P., ... Zheng, B. (2023). Global Carbon Budget 2023. Earth System Science Data, 15(12), 5301–
- 740 B., Alin, S. R., Anthoni, P., ... Zheng, B. (2023). Global Carbon Budget 2023. Earth System Science Data, 15(12), 5301–5369. https://doi.org/10.5194/essd-15-5301-2023
  - Gao, H., Schreiber, F., Collins, G., Jensen, M. M., Kostka, J. E., Lavik, G., De Beer, D., Zhou, H. Y., & Kuypers, M. M. M. (2010). Aerobic denitrification in permeable Wadden Sea sediments. *ISME Journal*, 4(3), 417–426. https://doi.org/10.1038/ismej.2009.127
- Gattuso, J. P., Frankignoulle, M., & Wollast, R. (1998). Carbon and carbonate metabolism in coastal aquatic ecosystems.

  Annual Review of Ecology and Systematics, 29(1998), 405–434. https://doi.org/10.1146/annurev.ecolsys.29.1.405
  - Gruber, N., Clement, D., Carter, B. R., Feely, R. A., van Heuven, S., Hoppema, M., Ishii, M., Key, R. M., Kozyr, A., Lauvset, S. K., Lo Monaco, C., Mathis, J. T., Murata, A., Olsen, A., Perez, F. F., Sabine, C. L., Tanhua, T., & Wanninkhof, R. (2019). The oceanic sink for anthropogenic CO 2 from 1994 to 2007. *Science*, 363(6432), 1193–1199. https://doi.org/10.1126/science.aau5153
  - Grunwald, M., Dellwig, O., Beck, M., Dippner, J. W., Freund, J. A., Kohlmeier, C., Schnetger, B., & Brumsack, H. J. (2009).

    Methane in the southern North Sea: Sources, spatial distribution and budgets. *Estuarine, Coastal and Shelf Science*, 81(4), 445–456. https://doi.org/10.1016/j.ecss.2008.11.021
- Herrling, G., & Winter, C. (2015). Tidally- and wind-driven residual circulation at the multiple-inlet system East Frisian

  Wadden Sea. Continental Shelf Research, 106, 45–59. https://doi.org/10.1016/j.csr.2015.06.001

- Hoppema, J. M. J. (1990). The distribution and seasonal variation of alkalinity in the Southern Bight of the North Sea and in the Western Wadden Sea. *Netherlands Journal of Sea Research*, 26(1), 11–23. https://doi.org/10.1016/0077-7579(90)90053-J
- Hu, X., & Cai, W. J. (2011). An assessment of ocean margin anaerobic processes on oceanic alkalinity budget. *Global Biogeochemical Cycles*, 25(3). https://doi.org/10.1029/2010GB003859
  - Jiang, L.-Q., Cai, W.-J., & Wang, Y. (2008). A comparative study of carbon dioxide degassing in river- and marine-dominated estuaries. *Limnology and Oceanography*, 53(6), 2603–2615. https://doi.org/10.4319/lo.2008.53.6.2603
  - Joesoef, A., Huang, W. J., Gao, Y., & Cai, W. J. (2015). Air-water fluxes and sources of carbon dioxide in the Delaware Estuary: Spatial and seasonal variability. *Biogeosciences*, 12(20), 6085–6101. https://doi.org/10.5194/bg-12-6085-2015
- Kamyshny, A., & Ferdelman, T. G. (2010). Dynamics of zero-valent sulfur species including polysulfides at seep sites on intertidal sand flats (Wadden Sea, North Sea). *Marine Chemistry*, 121(1–4), 17–26. https://doi.org/10.1016/j.marchem.2010.03.001

- Kieskamp, W., Lohse, L., Epping, E., & Helder, W. (1991). Seasonal variation in denitrification rates and nitrous oxide fluxes in intertidal sediments of the western Wadden Sea. *Marine Ecology Progress Series*, 72, 145–151. https://doi.org/10.3354/meps072145
- Kowalski, N., Dellwig, O., Beck, M., Gräwe, U., Neubert, N., Nägler, T. F., Badewien, T. H., Brumsack, H.-J., van Beusekom, J. E. E., & Böttcher, M. E. (2013). Pelagic molybdenum concentration anomalies and the impact of sediment resuspension on the molybdenum budget in two tidal systems of the North Sea. *Geochimica et Cosmochimica Acta*, 119, 198–211. https://doi.org/10.1016/j.gca.2013.05.046
- Kroeker, K. J., Kordas, R. L., Crim, R., Hendriks, I. E., Ramajo, L., Singh, G. S., Duarte, C. M., & Gattuso, J. P. (2013).
  Impacts of ocean acidification on marine organisms: Quantifying sensitivities and interaction with warming. *Global Change Biology*, 19(6), 1884–1896. https://doi.org/10.1111/gcb.12179
  - Lee, K., Kim, T.-W., Byrne, R. H., Millero, F. J., Feely, R. A., & Liu, Y.-M. (2010). The universal ratio of boron to chlorinity for the North Pacific and North Atlantic oceans. *Geochimica et Cosmochimica Acta*, 74(6), 1801–1811. https://doi.org/10.1016/j.gca.2009.12.027
  - Legge, O., Johnson, M., Hicks, N., Jickells, T., Diesing, M., Aldridge, J., Andrews, J., Artioli, Y., Bakker, D. C. E., Burrows, M. T., Carr, N., Cripps, G., Felgate, S. L., Fernand, L., Greenwood, N., Hartman, S., Kröger, S., Lessin, G., Mahaffey, C., ... Williamson, P. (2020). Carbon on the Northwest European Shelf: Contemporary Budget and Future Influences. Frontiers in Marine Science, 7. https://doi.org/10.3389/fmars.2020.00143
- Lehmann, N., Stacke, T., Lehmann, S., Lantuit, H., Gosse, J., Mears, C., Hartmann, J., & Thomas, H. (2023). Alkalinity responses to climate warming destabilise the Earth's thermostat. *Nature Communications*, 14(1). https://doi.org/10.1038/s41467-023-37165-w
  - Lewis, E., & Wallace, D. (1998). Program developed for CO{sub 2} system calculations. https://doi.org/10.2172/639712

- Li, X., Wu, Z., Ouyang, Z., & Cai, W.-J. (2024). The source and accumulation of anthropogenic carbon in the U.S. East Coast.

  Science Advances, 10(32), 3169. https://doi.org/10.1126/sciadv.adl3169
  - Liang, H., Lunstrum, A. M., Dong, S., Berelson, W. M., & John, S. G. (2023). Constraining CaCO3 Export and Dissolution With an Ocean Alkalinity Inverse Model. *Global Biogeochemical Cycles*, *37*(2). https://doi.org/10.1029/2022GB007535
  - Lorkowski, I., Pätsch, J., Moll, A., & Kühn, W. (2012). Interannual variability of carbon fluxes in the North Sea from 1970 to 2006 Competing effects of abiotic and biotic drivers on the gas-exchange of CO 2. *Estuarine, Coastal and Shelf Science*, 100, 38–57. https://doi.org/10.1016/j.ecss.2011.11.037

805

815

- Luebben, A., Dellwig, O., Koch, S., Beck, M., Badewien, T. H., Fischer, S., & Reuter, R. (2009). Distributions and characteristics of dissolved organic matter in temperate coastal waters (Southern North Sea). *Ocean Dynamics*, 59(2), 263–275. https://doi.org/10.1007/s10236-009-0181-x
- Macovei, V. A., Petersen, W., Brix, H., & Voynova, Y. G. (2021). Reduced Ocean Carbon Sink in the South and Central North

  Sea (2014–2018) Revealed From FerryBox Observations. *Geophysical Research Letters*, 48(11), 1–11.

  https://doi.org/10.1029/2021GL092645
  - NorbisrathMoore, W. S., Beck, M., Van Beusekom,Riedel, T., Rutgers van der Loeff, M., Dellwig, O., Shaw, T. J. E. E., & Thomas., Schnetger, B., & Brumsack, H. (2024a). Alkalinity sources J. (2011). Radium-based pore water fluxes of silica, alkalinity, manganese, DOC, and uranium: A decade of studies in the DutchGerman Wadden Sea. Ocean Science, 20(5), 1423–1440. Geochimica et Cosmochimica Acta, 75(21), 6535–6555. https://doi.org/10.5194/os-20-1423-20241016/j.gca.2011.08.037
  - Norbisrath, M., Van Beusekom, J. E. E., & Thomas, H. (2024b2024). Alkalinity sources in the Dutch Wadden Sea. *Ocean Science*, 20(5), 1423–1440. https://doi.org/10.5194/os-20-1423-2024
- Orr, J. C., Fabry, V. J., Aumont, O., Bopp, L., Doney, S. C., Feely, R. A., Gnanadesikan, A., Gruber, N., Ishida, A., Joos, F., Key, R. M., Lindsay, K., Maier-Reimer, E., Matear, R., Monfray, P., Mouchet, A., Najjar, R. G., Plattner, G. K., Rodgers, K. B., ... Yool, A. (2005). Anthropogenic ocean acidification over the twenty-first century and its impact on calcifying organisms. *Nature*, 437(7059), 681–686. https://doi.org/10.1038/nature04095
  - Pätsch, J., & Lenhart, H. (2004). Daily Loads of Nutrients, Total Alkalinity, Dissolved Inorganic Carbon and Dissolved Organic Carbon of the European Continental Rivers for the Years 1977-2002. https://doi.org/https://books.google.de/books?id=ubIPMQAACAAJ
  - Postma, H. (1981). Exchange of materials between the North Sea and the Wadden Sea. *Marine Geology*, 40(1–2), 199–213. https://doi.org/10.1016/0025-3227(81)90050-5
  - Prowe, A. E. F., Thomas, H., Pätsch, J., Kühn, W., Bozec, Y., Schiettecatte, L. S., Borges, A. V., & de Baar, H. J. W. (2009). Mechanisms controlling the air-sea CO2 flux in the North Sea. *Continental Shelf Research*, 29(15), 1801–1808. https://doi.org/10.1016/j.csr.2009.06.003
  - Redfield, A. C., Ketchum, B. H., & Richards, F. A. (1963). The influence of organisms on the composition of seawater. *The Sea*, 2, 26–77.

- Ricour, F., Guidi, L., Gehlen, M., DeVries, T., & Legendre, L. (2023). Century-scale carbon sequestration flux throughout the ocean by the biological pump. *Nature Geoscience*, 16(12), 1105–1113. https://doi.org/10.1038/s41561-023-01318-9
- Sabine, C. L., Feely, R. A., Gruber, N., Key, R. M., Lee, K., Bullister, J. L., Wanninkhof, R., Wong, C. S., Wallace, D. W. R., Tilbrook, B., Millero, F. J., Peng, T.-H., Kozyr, A., Ono, T., & Rios, A. F. (2004). The Oceanic Sink for Anthropogenic CO 2. Science, 305(5682), 367–371. https://doi.org/10.1126/science.1097403

- Santos, I. R., Beck, M., Brumsack, H. J., Maher, D. T., Dittmar, T., Waska, H., & Schnetger, B. (2015). Porewater exchange as a driver of carbon dynamics across a terrestrial-marine transect: Insights from coupled 222Rn and pCO2 observations in the German Wadden Sea. *Marine Chemistry*, 171, 10–20. https://doi.org/10.1016/j.marchem.2015.02.005
- Schmidt, C., Hanfland, C., Regnier, P., van Cappellen, P., Schlüter, M., Knauthe, U., Stimac, I., & Geibert, W. (2011). 228Ra, 226Ra, 224Ra and 223Ra in potential sources and sinks of land-derived material in the German Bight of the North Sea:

  Implications for the use of radium as a tracer. *Geo-Marine Letters*, 31(4), 259–269. https://doi.org/10.1007/s00367-011-0231-5
- 835 Schwichtenberg, F. (2013). Drivers of the carbonate system variability in the southern North Sea: River input, anaerobic alkalinity generation in the Wadden Sea and internal processes.
  - Schwichtenberg, F., Pätsch, J., Ernst Böttcher, M., Thomas, H., & Winde, V. (2020). The impact of intertidal areas on the carbonate system of the southern North Sea. *Biogeosciences*, 17(16), 4223–4245. https://doi.org/10.5194/bg-17-4223-2020
- Staneva, J., Stanev, E. V., Wolff, J. O., Badewien, T. H., Reuter, R., Flemming, B., Bartholomä, A., & Bolding, K. (2009).

  Hydroynamics and sediment dynamics in the German Bight. A focus on observations and numerical modelling in the

  East Frisian Wadden Sea. Continental Shelf Research, 29(1), 302–319. https://doi.org/10.1016/j.csr.2008.01.006
  - Thomas, H., Bozec, Y., Elkalay, K., <u>Dede</u> Baar, H. J. W., Borges, A. V<sub>5.2</sub> & Schiettecatte, L.-S. (2005). Controls of the surface water partial pressure of <u>CO-2CO2</u> in the North Sea. <u>In-Biogeosciences (Vol. 2)</u>. <u>www.biogeosciences.net</u>, <u>2(4)</u>, <u>323–334</u>. <u>https://doi.org/10.5194/bg/\_2/-323/SRef ID:1726-4189/bg/\_2005-2-323EuropeanGeosciencesUnion</u>
  - Thomas, H., Prowe, A. E. F., van Heuven, S., Bozec, Y., de Baar, H. J. W., Schiettecatte, L. S., Suykens, K., Koné, M., Borges, A. V., Lima, I. D., & Doney, S. C. (2007). Rapid decline of the CO2 buffering capacity in the North Sea and implications for the North Atlantic Ocean. *Global Biogeochemical Cycles*, 21(4). https://doi.org/10.1029/2006GB002825
- Thomas, H., Schiettecatte, L.-S., Suykens, K., Koné, Y. J. M., Shadwick, E. H., Prowe, A. E. F., Bozec, Y., De Baar, H. J. W., & 850 Borges, A.-V. (2009). Enhanced ocean carbon storage from anaerobic alkalinity generation in coastal sediments. In Biogeosciences (Vol. 6). www.biogeosciences.net/6/267/2009/
  - Thomas, H., Schiettecatte, L. S., Suykens, K., Koné, Y. J. M., Shadwick, E. H., Prowe, A. E. F., Bozec, Y., de Baar, H. J. W., & Borges, A. V. (2009). Enhanced ocean carbon storage from anaerobic alkalinity generation in coastal sediments. *Biogeosciences*, 6(2), 267–274. https://doi.org/10.5194/bg-6-267-2009
- 855 UNESCO World Heritage Centre, & accessed 23 March 2025. (n.d.). The Wadden Sea. (N.d.).

- Van Beusekom, J. E. E., Brockmann, U. H., Hesse, K.-J., Hickel, W., Poremba, K., & Tillmann, U. (1999). The importance of sediments in the transformation and turnover of nutrients and organic matter in the Wadden Sea and German Bight. Deutsche Hydrographische Zeitschrift, 51(2–3), 245–266. https://doi.org/10.1007/BF02764176
- Van Beusekom, J. E. E., Buschbaum, C., & Reise, K. (2012). Wadden Sea tidal basins and the mediating role of the North Sea in ecological processes: scaling up of management? *Ocean & Coastal Management*, 68, 69–78. https://doi.org/10.1016/j.ocecoaman.2012.05.002
  - Van Beusekom, J. E. E., & De Jonge, V. N. (2002). Long-term changes in Wadden Sea nutrient cycles: Importance of organic matter import from the North Sea. *Hydrobiologia*, 475–476, 185–194. https://doi.org/10.1023/A:1020361124656
- Voynova, Y. G., Petersen, W., Gehrung, M., Aßmann, S., & King, A. L. (2019). Intertidal regions changing coastal alkalinity:

  The Wadden Sea-North Sea tidally coupled bioreactor. *Limnology and Oceanography*, 64(3), 1135–1149. https://doi.org/10.1002/lno.11103
  - Wolf-Gladrow, D. A., Zeebe, R. E., Klaas, C., Körtzinger, A., & Dickson, A. G. (2007). Total alkalinity: The explicit conservative expression and its application to biogeochemical processes. *Marine Chemistry*, 106(1-2 SPEC. ISS.), 287–300. https://doi.org/10.1016/j.marchem.2007.01.006
- Wu, C. S., Røy, H., & de Beer, D. (2015). Methanogenesis in sediments of an intertidal sand flat in the Wadden Sea. *Estuarine, Coastal and Shelf Science*, 164, 39–45. <a href="https://doi.org/10.1016/j.ecss.2015.06.031">https://doi.org/10.1016/j.ecss.2015.06.031</a>

- Xue, L., Cai, W. J., Sutton, A. J., & Sabine, C. (2017). Sea surface aragonite saturation state variations and control mechanisms at the Gray's Reef time-series site off Georgia, USA (2006–2007). *Marine Chemistry*, 195, 27–40. https://doi.org/10.1016/j.marchem.2017.05.009
- Xue, L., & Cai, W. J. (2020). Total alkalinity minus dissolved inorganic carbon as a proxy for deciphering ocean acidification mechanisms. *Marine Chemistry*, 222. https://doi.org/10.1016/j.marchem.2020.103791